SIAM J. SCI. COMPUT.
Vol. 46, No. 2, pp. A1252–A1275

APPROXIMATING THE SHAPE OPERATOR WITH THE SURFACE HELLAN–HERRMANN–JOHNSON ELEMENT*

SHAWN W. WALKER†

Abstract. We present a finite element technique for approximating the surface Hessian of a discrete scalar function on triangulated surfaces embedded in $\mathbb{R}^3$, with or without boundary. We then extend the method to compute approximations of the full shape operator of the underlying surface using only the known discrete surface. The method is based on the Hellan–Herrmann–Johnson element and does not require any ad hoc modifications. Convergence is established provided the discrete surface satisfies a Lagrange interpolation property related to the exact surface. The convergence rate, in L^2, for the shape operator approximation is $O(h^m)$, where $m \geq 1$ is the polynomial degree of the surface, i.e., the method converges even for piecewise linear surface triangulations. For surfaces with boundary, some additional boundary data is needed to establish optimal convergence, e.g., boundary information about the surface normal vector or the curvature in the co-normal direction. Numerical examples are given on nontrivial surfaces that demonstrate our error estimates and the efficacy of the method.

Key words. surface Hessian, shape operator, surface finite elements, open surfaces, geometric consistency error

MSC codes. 65D18, 65N30, 68U05

DOI. 10.1137/22M1531968

1. Introduction.

Approximating curvatures from discrete surfaces has a long history in computer graphics and computational geometry, e.g., in computer-aided geometric modeling [45, 42, 46], feature detection/extraction [25, 6], surface fairing and mesh smoothing [14, 36, 32, 31], and reparameterizing surfaces for texturing and remeshing [46, 23]. Often, one needs estimates of normal vectors and curvature information at mesh vertices, which has spawned many discrete schemes based on local (weighted) averages, e.g., the well-known co-tangent formula for the mean curvature vector [30, 20] and discrete Laplace–Beltrami operators [9, 16, 15], as well as schemes to approximate the Gaussian curvature of discrete surfaces using local formulas [43].

The convergence of these schemes, for sequences of refined meshes converging to the underlying (smooth) surface, is well-studied. Indeed, it is known that any numerical scheme that uses the 1-ring neighborhood of a vertex to compute curvature *does not converge* for general, piecewise linear meshes [20, 44]. For special meshes, one can construct schemes that do converge (see [43, 7]). Other approaches include surface fitting techniques [35, 18, 20, 34, 21] that construct polynomial surface "patches" over the triangulation, which can be directly differentiated to yield accurate curvature information. However, computing with patches is not trivial, involves complicated procedures, and depends on the mesh quality (see [19] for unstructured simplex splines on flat domains).

Other approaches utilize finite element techniques. For instance, using a higher order approximation of the surface, e.g., a piecewise quadratic triangulation, yields a convergent approximation of the curvature [24]. In fact, one can just directly compute

*Submitted to the journal's Numerical Algorithms for Scientific Computing section October 31, 2022; accepted for publication (in revised form) December 21, 2023; published electronically April 8, 2024.

https://doi.org/10.1137/22M1531968

Funding: This work was funded by NSF DMS-2111474.

†Department of Mathematics, Louisiana State University, Baton Rouge, LA 70803 USA (walker@math.lsu.edu).

the shape operator of the surface on each (curved) triangle in the mesh. See also [22] for higher order approximation of Gaussian curvature with Regge elements. But in many applications, only piecewise linear surface triangulations are available.

This paper presents a novel technique that utilizes the surface Hellan–Herrmann–Johnson (HHJ) method, originally developed for the surface Kirchhoff plate equation in [40], as a postprocessing scheme to approximate the surface Hessian of a scalar function. Furthermore, we show that this scheme can be used to approximate the *full shape operator* of the surface, which is our main goal. For closed, *piecewise linear* surface triangulations, whose vertices lie on the true surface, the method yields an approximation that is *provably first-order* accurate in the L^2 norm, i.e., $O(h)$, where h is the maximum diameter of mesh elements. For surfaces with boundary, some additional information is needed at the boundary; otherwise the accuracy degrades to $O(h^{1/2})$ near the boundary. The method essentially consists of a matrix-vector product that computes a nonconforming surface Hessian of the mesh coordinates, followed by an L^2-like projection to an HHJ element. Heuristically, the method uses information over neighboring mesh elements (through jumps in the tangent space) to obtain an approximation of the curvature. The method also generalizes to higher order triangulations, with $O(h^m)$ accuracy, where m is the polynomial degree of the triangulation, as long as a moment based, Lagrange interpolation of the surface is used (see (4.2) and (4.14)). To the best of our knowledge, no other finite element method can do this. Moreover, the lowest order version of the method is simple to implement. Given an approximation of the shape operator, it is then trivial to compute the principle curvatures and principle directions of the surface.

Section 2 gives the basic background for working on surfaces. In section 3, we describe a nonconforming formulation for approximating the surface Hessian of a scalar function by an L^2 like projection and discuss the tools for dealing with curved, parametric surface approximations. In particular, Theorem 3.5 is a crucial extension of [40, Thm. 4.8]. Section 4 gives the finite element scheme for the L^2 projection of the surface Hessian and performs the main error analysis that includes the geometric error of the surface approximation. Next, we describe our scheme for approximating the shape operator of the exact surface in section 5, which utilizes an important identity in Proposition 5.1, and discuss the details of its practical computation. Section 6 presents several numerical results illustrating the method on surfaces with and without boundary. We close with some remarks in section 7. The supplementary material (123872_1_supp_541500_s1c356_sc.pdf [local/web 230KB]) provides an overview of essential differential geometry concepts.

2. A surface FEM for the surface Hessian.

2.1. Surface definitions. Let Γ be a C^p connected, two-dimensional manifold embedded in $\mathbb{R}^3$, where $p \geq 2$. If Γ has a boundary $\partial\Gamma := \Sigma$, we assume Σ is piecewise C^p with a finite number of corners, with interior angle $\alpha_i \in (0, 2\pi]$ of the ith corner measured with respect to the Euclidean metric in $\mathbb{R}^3$ (see Figure 1). In particular, Σ is globally continuous and parameterized by a piecewise curve. In addition, we assume $\Sigma = \overline{\Sigma_{\mathrm{c}}} \cup \overline{\Sigma_{\mathrm{s}}}$ partitions into two mutually disjoint, one-dimensional open sets Σ_{c} (clamped) and Σ_{s} (simply supported); either set can be empty.

We note some facts from section SM2. Let $\mathrm{id}_\Gamma : \Gamma \to \Gamma$ be the identity map, i.e., $\mathbf{x} = \mathrm{id}_\Gamma(\mathbf{x})$ for all $\mathbf{x} \in \Gamma$, and let $\boldsymbol{\nu} : \Gamma \to \mathbb{R}^3$ be the (locally defined) unit normal vector of Γ. The tangent space projection $\boldsymbol{P} : \mathbb{R}^3 \to \mathbb{R}^3$, defined on Γ, is given by $\boldsymbol{P} = \boldsymbol{I} - \boldsymbol{\nu} \otimes \boldsymbol{\nu}$ (see (SM2.1)) and satisfies the identity $\nabla_\Gamma \mathrm{id}_\Gamma = \boldsymbol{P}$ (see subsection 2.2 for ∇_Γ). Given a vector $\mathbf{v} \in \mathbb{R}^3$, it is in the tangent space $T_{\mathbf{x}}(\Gamma)$ if $\boldsymbol{P}(\mathbf{x})\mathbf{v} = \mathbf{0}$. We

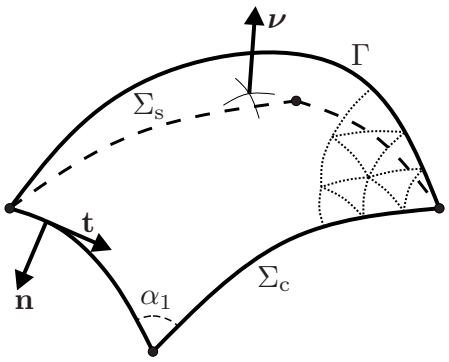

FIG. 1. *Illustration of curved surface* Γ *in* $\mathbb{R}^3$ *with mesh. The boundary* $\Sigma \equiv \partial\Gamma$ *decomposes as* $\Sigma = \overline{\Sigma_c} \cup \overline{\Sigma_s}$ *and has a finite number of corners with interior angles* α_i*. The boundary* Σ *has (outer) conormal vector,* $\boldsymbol{n}$*, and oriented unit tangent vector,* $\boldsymbol{t}$*. The normal vector of* Γ *is* $\boldsymbol{\nu}$*. Part of the exact, curved surface triangulation* $\mathcal{T}_h$ *is shown with dotted curves.*

define the tangent bundle: $T(\Gamma) = \{(\mathbf{x}, \mathbf{v}) \,|\, \mathbf{x} \in \Gamma,\, \mathbf{v}(\mathbf{x}) \in T_{\mathbf{x}}(\Gamma)\}$. So, we say $\mathbf{v} \in T(\Gamma)$ if $\mathbf{v}(\mathbf{x}) \in T_{\mathbf{x}}(\Gamma)$ for every $\mathbf{x} \in \Gamma$; in this case, we write $\mathbf{v} : \Gamma \to T(\Gamma)$.

Next, let $\mathbb{R}^{3\times 3}$ be the space of (extrinsic) 2-tensors in three dimensions, and define the subset of tensors on the tangent bundle of Γ,

$$\mathbf{T} \equiv \mathbf{T}(\Gamma) := \{\boldsymbol{\varphi} : \Gamma \to \mathbb{R}^{3\times 3} \,|\, \boldsymbol{P}\boldsymbol{\varphi} \equiv \boldsymbol{\varphi},\, \boldsymbol{P}\boldsymbol{\varphi}^T \equiv \boldsymbol{\varphi}^T\}, \tag{2.1}$$

and define the set of symmetric tensors on the tangent bundle of Γ:

$$\mathbf{S} \equiv \mathbf{S}(\Gamma) := \{\boldsymbol{\varphi} \in \mathbf{T}(\Gamma) \,|\, \boldsymbol{\varphi} = \boldsymbol{\varphi}^T\}. \tag{2.2}$$

2.2. Differential operators on surfaces. Let $v : \Gamma \to \mathbb{R}$ be a smooth function defined on Γ. We call $\nabla_\Gamma v \equiv \operatorname{grad}_\Gamma v : \Gamma \to T(\Gamma)$ the surface gradient of v (see (SM2.2)) and $\nabla_\Gamma \nabla_\Gamma w \equiv \operatorname{hess}_\Gamma w : \Gamma \to \mathbf{S}(\Gamma)$ the surface Hessian of v (see (SM2.3)). Moreover, we have the function space $L^2(\Gamma) := \{v : \Gamma \to \mathbb{R} \mid \int_\Gamma |v|^2 d\mathrm{S} < \infty\}$, with inner product $(w, v)_{L^2(\Gamma)} := \int_\Gamma wv\, d\mathrm{S}$ and norm $\|v\|^2_{L^2(\Gamma)} := (v, v)_{L^2(\Gamma)}$, as well as the Sobolev (Hilbert) spaces $H^1(\Gamma) := \{v \in L^2(\Gamma) \,|\, \|\nabla_\Gamma v\|_{L^2(\Gamma)} < \infty\}$ and $H^2(\Gamma) := \{v \in H^1(\Gamma) \,|\, \|\nabla_\Gamma \nabla_\Gamma v\|_{L^2(\Gamma)} < \infty\}$, with inner products given by

$$\begin{aligned} (w, v)_{H^1(\Gamma)} &:= \int_\Gamma wv + \nabla_\Gamma w \cdot \nabla_\Gamma v\, d\mathrm{S}, \\ (w, v)_{H^2(\Gamma)} &:= (w, v)_{H^1(\Gamma)} + \int_\Gamma \nabla_\Gamma \nabla_\Gamma w : \nabla_\Gamma \nabla_\Gamma v\, d\mathrm{S}, \end{aligned} \tag{2.3}$$

and corresponding norms $\|v\|^2_{H^1(\Gamma)} := (v, v)_{H^1(\Gamma)}$, $\|v\|^2_{H^2(\Gamma)} := (v, v)_{H^2(\Gamma)}$. Other types of Sobolev spaces are defined in an analogous way.

We denote by $\mathring{H}^\ell(\Gamma) \subset H^\ell(\Gamma)$ the Sobolev space with vanishing boundary conditions up to degree $\ell - 1$. We will need the subspace of $H^2(\Gamma)$,

$$\mathcal{W}(\Gamma) := \{w \in H^2(\Gamma) \,|\, w = 0,\ \text{on } \Sigma,\ \boldsymbol{n} \cdot \nabla_\Gamma w = 0,\ \text{on } \Sigma_c\} \text{ if } \Sigma \neq \emptyset, \tag{2.4}$$

and $\mathcal{W}(\Gamma) = H^2(\Gamma)$ when $\Sigma = \emptyset$. In addition, we have $\mathcal{V}(\Gamma) := L^2(\Gamma; \mathbf{S}(\Gamma))$.

2.3. Projection of the surface Hessian. Given $w \in \mathcal{W}$, we define $\boldsymbol{\sigma} \in \mathcal{V}$ such that

$$(\boldsymbol{\sigma}, \boldsymbol{\tau})_{L^2(\Gamma)} = (\nabla_\Gamma \nabla_\Gamma w, \boldsymbol{\tau})_{L^2(\Gamma)} \quad \forall\, \boldsymbol{\tau} \in \mathcal{V}, \tag{2.5}$$

i.e., $\boldsymbol{\sigma}$ is the L^2 projection of $\nabla_\Gamma \nabla_\Gamma w$, which means $\boldsymbol{\sigma} = \nabla_\Gamma \nabla_\Gamma w$ a.e. in Γ. The presence of vanishing boundary conditions in $\mathcal{W}$ is not critical; one can pose (2.5) for any $w \in H^2(\Gamma)$. However, the method we develop handles the slope condition in (2.4) as a *natural* condition, so we keep (2.5) as stated. In subsection 3.4, we show how to handle inhomogeneous boundary conditions.

3. Nonconforming formulation of the surface Hessian. Major difficulties arise in solving (2.5) if the surface is only continuous, piecewise smooth, as well as when the data w is only a discrete, finite element function. In order to circumvent these difficulties, and obtain a convergent approximation of the surface Hessian of a discrete function w posed on a discrete surface, we adopt a nonconforming approach that is first built on a mesh-dependent version of $H^2(\Gamma)$. This then leads to the surface version of the HHJ element (see [40]), which is used to approximate the $\boldsymbol{\sigma}$ variable in (2.5). See also [10, 5, 4, 8, 3] for analysis of the classic HHJ element. The initial idea is to triangulate Γ and define infinite dimensional, mesh-dependent spaces on that triangulation.

3.1. Curved triangulations. We start with a conforming, shape regular, piecewise linear triangulation $\mathcal{T}_h^1 = \{T^1\}$ of a polyhedral domain Γ^1 that interpolates Γ at the vertices; furthermore, the boundary vertices of Γ^1 (namely Σ^1) lie on the boundary of Γ. See [13, 12, 17, 15, 40] for more discussion on how this triangulation can be generated. Let $\mathcal{T}_{\partial,h}^1$ be the set of triangles with one side on Σ^1 and, for convenience, assume the triangulation satisfies the following technical property (see [40]).

PROPERTY 1. *Each triangle in $\mathcal{T}_h^1$ has at most two vertices on the boundary and so has at most one edge contained in Σ^1.*

We assume $\mathcal{T}_h^1$ is homeomorphic to an exact triangulation $\mathcal{T}_h = \{T\}$ of Γ. Specifically, we assume there exists a homeomorphic mapping $\boldsymbol{F} : \Gamma^1 \to \Gamma$ such that $\boldsymbol{F}_T \equiv \boldsymbol{F}|_{T^1}$ is a diffeomorphism from $T^1 \in \mathcal{T}_h^1$ to an exact (curved) triangle $T \in \mathcal{T}_h$. The map $\boldsymbol{F}$ can be defined using a parametrization of the surface or through the closest point projection (see [15, 17] for more details). Moreover, as $h \to 0$, we assume the discrete normal $\boldsymbol{\nu}_h$ of Γ^1 converges to the exact normal $\boldsymbol{\nu}$ of Γ, i.e., $\|\boldsymbol{\nu}_h \circ \boldsymbol{F}^{-1} - \boldsymbol{\nu}\|_{L^\infty(\Gamma)} = O(h)$; cf. [26, sect. 36, 37, pp. 111–117].

We generate higher order approximations Γ^m of Γ by simply interpolating $\boldsymbol{F}$ over Γ^1 with degree m Lagrange polynomials, i.e., we have the map $\boldsymbol{F}^m : \Gamma^1 \to \Gamma^m$ given by $\boldsymbol{F}^m := \mathcal{I}_h^{1,m} \boldsymbol{F}$, where $\mathcal{I}_h^{1,m}$ is the Lagrange interpolation operator of degree m given in subsection 4.1, or the standard nodal interpolant can be used. Note that $\boldsymbol{F}_T^1 \equiv \mathrm{id}_{T^1}$. We emphasize that $\boldsymbol{F}$ is only needed for theoretical reasons, such as in the error analysis (see (4.14)). For instance, the numerical schemes in (4.9) and (5.11) can be applied on any given degree m surface Γ^m.

We also have maps between approximate domains of degrees l and m by

$$\boldsymbol{\Phi}^{lm}|_T = \boldsymbol{\Phi}_T^{lm} : T^l \to T^m, \text{ where } \boldsymbol{\Phi}_T^{lm} := \boldsymbol{F}_T^m \circ (\boldsymbol{F}_T^l)^{-1}, \text{ so } \boldsymbol{\Phi}_T^{1m} \equiv \boldsymbol{F}_T^m. \tag{3.1}$$

We also require a map from the approximate domain Γ^m to the exact domain Γ. Specifically, given a triangle $T^m \in \mathcal{T}_h^m$, we define a diffeomorphism $\boldsymbol{\Psi}_T^m : T^m \to T \in \mathcal{T}_h$ by $\boldsymbol{\Psi}_T^m := \boldsymbol{F}_T \circ (\boldsymbol{F}_T^m)^{-1}$, so then $\mathcal{T}_h \equiv \{\boldsymbol{\Psi}_T^m(T^m)\}_{T^m \in \mathcal{T}_h^m}$. The $\boldsymbol{\Psi}_T^m$ may be pieced together to give a global map $\boldsymbol{\Psi}^m : \Gamma^m \to \Gamma$. In addition, it is assumed that the discrete normal of Γ^m converges with order m, i.e., $\|\boldsymbol{\nu}_h \circ (\boldsymbol{\Psi}^m)^{-1} - \boldsymbol{\nu}\|_{L^\infty(\Gamma)} = O(h^m)$ (provided Γ is at least C^{m+1}).

The notation Γ and Γ^m is inconvenient because the exact domain has no superscript, but the polynomial approximation does. Thus, for convenience in later

statements, we will abuse notation and make the identification $\Gamma^\infty \equiv \Gamma$, $\mathcal{T}_h^\infty \equiv \mathcal{T}_h$, $\boldsymbol{\Phi}^{l\infty} \equiv \boldsymbol{\Psi}^l$, $\boldsymbol{F}_T^\infty \equiv \boldsymbol{\Psi}^1$, etc. This is motivated by the fact that for most C^∞ surfaces Γ, the polynomial approximate domain Γ^m, with triangulation $\mathcal{T}_h^m$, would converge to Γ as $m \to \infty$ with h *fixed.* Of course, we do not claim (in general) that Γ^m converges Γ, for fixed h, as $m \to \infty$, especially when Γ is not C^∞.

Thus, $\mathcal{T}_h^m$ is a conforming, shape regular triangulation that approximates Γ by $\Gamma^m := \bigcup_{T^m \in \mathcal{T}_h^m} \overline{T^m}$ for all $m \geq 1$ (where $\overline{G}$ is the closure of the set G). Next, we have the *skeleton* of the mesh, i.e., the set of (curved) mesh edges $\mathcal{E}_h^m := \partial \mathcal{T}_h^m$. Let $\mathcal{E}_{\partial,h}^m \subset \mathcal{E}_h^m$ denote the subset of edges that are contained in the boundary $\Sigma^m = \partial \Gamma^m$ and respect the boundary partition of Σ^m. The internal edges are given by $\mathcal{E}_{0,h}^m := \mathcal{E}_h^m \setminus \mathcal{E}_{\partial,h}^m$. We assume the meshes are quasi-uniform and shape regular [11], with mesh size $h := \max_T h_T$, where $h_T := \operatorname{diam}(T)$ for any $T \in \mathcal{T}_h$. We also assume the corners of Σ are captured by vertices of the mesh.

The main approximation properties for these maps are summarized in the next theorem (see [40, Thm. 4.1]).

THEOREM 3.1. *Suppose Γ is a C^p surface for some fixed $p \geq 2$ (see* [1, Para. 4.10]*). Then, for all $1 \leq l \leq m \leq p-1$, or $1 \leq l \leq p-1$ and $m = \infty$ (see notation above), the maps $\boldsymbol{F}_T^m$, $\boldsymbol{F}_T^l$ described above satisfy*

$$\begin{aligned} &\|\nabla_{T^1}^s (\boldsymbol{F}_T^l - \mathrm{id}_{T^1})\|_{L^\infty(T^1)} \leq C h^{2-s} \quad \text{for } s = 0, 1, 2, \\ &\|\nabla_{T^1}^s (\boldsymbol{F}_T^m - \boldsymbol{F}_T^l)\|_{L^\infty(T^1)} \leq C h^{l+1-s} \quad \text{for } 0 \leq s \leq l+1, \\ &1 - Ch \leq \|[\nabla_{T^1} \boldsymbol{F}_T^l]^{-1}\|_{L^\infty(T^1)} \leq 1 + Ch, \quad \|[\nabla_{T^1} \boldsymbol{F}_T^l]^{-1} - \boldsymbol{I}\|_{L^\infty(T^1)} \leq Ch, \end{aligned} \tag{3.2}$$

where all constants depend on the C^{l+1} norm of Γ.

Next, recall the tangent $\boldsymbol{t}$, co-normal $\boldsymbol{n}$, and surface normal vectors $\boldsymbol{\nu}$ from Figure 1 and let $\tilde{\cdot}$, $\hat{\cdot}$, or $\bar{\cdot}$ denote quantities defined on T^s, or using $\boldsymbol{F}_T^s$, for $s = m$, l, or 1, respectively; e.g., $\tilde{\boldsymbol{\nu}}$ is the surface normal of T^m. Then, the following estimate holds:

$$\begin{aligned} \|\tilde{\boldsymbol{t}} \circ \boldsymbol{F}_T^m - \hat{\boldsymbol{t}} \circ \boldsymbol{F}_T^l\|_{L^\infty(T^1)} + \|\tilde{\boldsymbol{n}} \circ \boldsymbol{F}_T^m - \hat{\boldsymbol{n}} \circ \boldsymbol{F}_T^l\|_{L^\infty(T^1)} \\ + \|\tilde{\boldsymbol{\nu}} \circ \boldsymbol{F}_T^m - \hat{\boldsymbol{\nu}} \circ \boldsymbol{F}_T^l\|_{L^\infty(T^1)} \leq C h^l. \end{aligned} \tag{3.3}$$

3.2. Skeleton spaces. The spaces in this section are infinite dimensional, but "mesh dependent" (see [40]), and were originally motivated by [5, p. 1043] and [3, eq. (2.11)]. In defining the spaces and norms, we only consider the exact triangulation $\mathcal{T}_h$, but everything generalizes to the polynomial triangulations $\mathcal{T}_h^m$ in the obvious way. We make use of standard dG notation for writing inner products and norms over the triangulation, e.g., $(f,g)_{\mathcal{T}_h} := \sum_{T \in \mathcal{T}_h} (f,g)_T$, $\|f\|_{L^p(\mathcal{T}_h)}^p := \sum_{T \in \mathcal{T}_h} \|f\|_{L^p(T)}^p$, etc.

A mesh-dependent version of $H^2(\Gamma)$ is given by

$$H_h^2(\Gamma) := \{v \in H^1(\Gamma) \mid v|_T \in H^2(T) \text{ for } T \in \mathcal{T}_h\} \tag{3.4}$$

with the following seminorm:

$$\|v\|_{2,h}^2 := \|\nabla_\Gamma \nabla_\Gamma v\|_{L^2(\mathcal{T}_h)}^2 + h^{-1} \|[\![\boldsymbol{n} \cdot \nabla_\Gamma v]\!]\|_{L^2(\mathcal{E}_{0,h})}^2 + h^{-1} \|[\![\boldsymbol{n} \cdot \nabla_\Gamma v]\!]\|_{L^2(\Sigma_c)}^2, \tag{3.5}$$

where $[\![\eta]\!]$ is the jump in quantity η across mesh edge E, and $\boldsymbol{n}$ is the unit co-normal on $E \in \mathcal{E}_h$. Hence, if the edge E is shared by two triangles T_1 and T_2 with outward co-normals $\boldsymbol{n}_1$ and $\boldsymbol{n}_2$, then $[\![\boldsymbol{n} \cdot \nabla_\Gamma v]\!] = \boldsymbol{n}_1 \cdot \nabla_\Gamma v|_{T_1} + \boldsymbol{n}_2 \cdot \nabla_\Gamma v|_{T_2}$ on E. For E a boundary edge, we set $[\![\eta]\!] = \eta|_E$. We note the following norm equivalence when

mapping between domains Γ^m and Γ^l [40, eq. (4.9)]. Let $u \in H_h^2(\Gamma^m)$ and define $\hat{u} = u \circ \boldsymbol{\Phi}^{lm} \in H_h^2(\Gamma^l)$. Then, for $h > 0$ sufficiently small, $\|u\|_{2,h,m} \approx \|\hat{u}\|_{2,h,l}$, where $\|\cdot\|_{2,h,m}$ is (3.5) defined on Γ^m.

Next, for any $\boldsymbol{\varphi} \in H^1(\Gamma;\mathbf{S})$, define

$$\|\boldsymbol{\varphi}\|_{0,h}^2 := \|\boldsymbol{\varphi}\|_{L^2(\Gamma)}^2 + h\left\|\boldsymbol{n}^T\boldsymbol{\varphi}\boldsymbol{n}\right\|_{L^2(\mathcal{E}_{0,h})}^2 + h\left\|\boldsymbol{n}^T\boldsymbol{\varphi}\boldsymbol{n}\right\|_{L^2(\Sigma_c)}^2, \tag{3.6}$$

and define H_h^0 to be the completion: $H_h^0(\Gamma;\mathbf{S}) := \overline{H^1(\Gamma;\mathbf{S})}^{\|\cdot\|_{0,h}}$. By the definition of the norm, $H_h^0(\Gamma;\mathbf{S}) \equiv L^2(\Gamma;\mathbf{S}) \oplus L^2(\mathcal{E}_h;\mathbb{R})$, i.e., $\boldsymbol{\varphi} \in H_h^0(\Gamma;\mathbf{S})$ is actually $\boldsymbol{\varphi} \equiv (\boldsymbol{\varphi}', \varphi^{\mathrm{nn}})$, where $\boldsymbol{\varphi}' \in L^2(\Gamma;\mathbf{S})$ and $\varphi^{\mathrm{nn}} \in L^2(\mathcal{E}_h;\mathbb{R})$, with (in general) no connection between $\boldsymbol{\varphi}'$ and φ^{nn}. Note that if $\boldsymbol{\varphi} \in H^1(\Gamma;\mathbf{S}) \subset H_h^0(\Gamma;\mathbf{S})$, then $\boldsymbol{n}^T\boldsymbol{\varphi}'\boldsymbol{n}|_{\mathcal{E}_h} = \varphi^{\mathrm{nn}}$ (see [5] and [3]), i.e., the conormal-conormal trace of $\boldsymbol{\varphi}'$ on mesh edges agrees with φ^{nn}.

3.3. Mixed skeleton formulation. We introduce the skeleton subspaces

$$\mathcal{W}_h(\Gamma) := H_h^2(\Gamma) \cap \mathring{H}^1(\Gamma), \quad \mathcal{V}_h(\Gamma) := \{\boldsymbol{\varphi} \in H_h^0(\Gamma;\mathbf{S}) \mid \varphi^{\mathrm{nn}} = 0 \text{ on } \Sigma_s\} \tag{3.7}$$

when $\Sigma \neq \emptyset$, and $\mathcal{W}_h(\Gamma) := H_h^2(\Gamma)$, $\mathcal{V}_h(\Gamma) := H_h^0(\Gamma;\mathbf{S})$ when $\Sigma = \emptyset$; $\mathcal{W}_h$ and $\mathcal{V}_h$ are mesh-dependent versions of $\mathcal{W}$ and $\mathcal{V}$, respectively.

The nonconforming version of (2.5) is as follows, which is based on [40, eq. (3.10)]. For all $\boldsymbol{\varphi} \in H_h^0(\Gamma;\mathbf{S})$ and $v \in H_h^2(\Gamma)$, define

$$b_h(\boldsymbol{\varphi}, v) := -\sum_{T\in\mathcal{T}_h} (\boldsymbol{\varphi}, \mathrm{hess}_\Gamma v)_T + \sum_{E\in\mathcal{E}_h} \langle \varphi^{\mathrm{nn}}, [\![\boldsymbol{n}\cdot\nabla_\Gamma v]\!]\rangle_E, \tag{3.8}$$

where $[\![\boldsymbol{n}\cdot\nabla_\Gamma v]\!]|_E \equiv \boldsymbol{n}\cdot\nabla_\Gamma v$ when $E \subset \Sigma$, and $b_h(\boldsymbol{\varphi}, v)$ satisfies the continuity estimate: $b_h(\boldsymbol{\varphi}, v) \le \|\boldsymbol{\varphi}\|_{0,h}\|v\|_{2,h}$ for all $\boldsymbol{\varphi} \in \mathcal{V}_h$ and $v \in \mathcal{W}_h$. Next, define

$$a(\boldsymbol{\tau}, \boldsymbol{\varphi}) := (\boldsymbol{\tau}, \boldsymbol{\varphi})_\Gamma \quad \forall\, \boldsymbol{\tau}, \boldsymbol{\varphi} \in H_h^0(\Gamma;\mathbf{S}). \tag{3.9}$$

If $w \in \mathcal{W} \subset \mathcal{W}_h(\Gamma)$ and we set $\boldsymbol{\sigma} := \nabla_\Gamma\nabla_\Gamma w$, then $\boldsymbol{\sigma}$ and w satisfy

$$a(\boldsymbol{\sigma}, \boldsymbol{\varphi}) + b_h(\boldsymbol{\varphi}, w) = 0 \quad \forall\, \boldsymbol{\varphi} \in \mathcal{V}_h. \tag{3.10}$$

Note that the jump terms in (3.8) vanish because $w \in \mathcal{W}$ and $\boldsymbol{n}\cdot\nabla_\Gamma w = 0$ on Σ_c. Indeed, restricting $\boldsymbol{\varphi} = \boldsymbol{\sigma}$, then we have

$$\|\boldsymbol{\sigma}\|_{L^2(\Gamma)}^2 = a(\boldsymbol{\sigma}, \boldsymbol{\sigma}) = -b_h(\boldsymbol{\sigma}, w) \le \|\boldsymbol{\sigma}\|_{L^2(\Gamma)}\|\nabla_\Gamma\nabla_\Gamma w\|_{L^2(\Gamma)}, \tag{3.11}$$

so $\boldsymbol{\sigma}$ is the stable $L^2(\Gamma)$ projection of $\nabla_\Gamma\nabla_\Gamma w$.

Remark 3.2. We also have $\mathcal{W}_h(\Gamma^m) := H_h^2(\Gamma^m) \cap \mathring{H}^1(\Gamma^m)$ and $\mathcal{V}_h(\Gamma^m) := \{\boldsymbol{\varphi} \in H_h^0(\Gamma^m;\mathbf{S}) \mid \varphi^{\mathrm{nn}} = 0 \text{ on } \Sigma_s^m\}$ defined on the curved triangulation Γ^m, with associated forms $b_h^m(\boldsymbol{\varphi}, v)$, $a^m(\boldsymbol{\tau}, \boldsymbol{\varphi})$ defined on Γ^m in the obvious way. These will be used in our fully discrete version of (3.10) (see (4.7)), which will enable our method for approximating the surface Hessian of a discrete function.

3.4. Inhomogeneous boundary conditions. We extend the above formulation (3.10) to handle nonvanishing boundary conditions, which is necessary for approximating the shape operator on surfaces with boundary. First, assume that $w \in H^3(\Gamma)$ and there exists a function $g \in H^3(\Gamma)$ such that $w = g$ on Σ and $\partial_{\boldsymbol{n}} w = \partial_{\boldsymbol{n}} g$ on Σ_c. Next, construct a function $\boldsymbol{\rho} \in H^1(\Gamma;\mathbf{S})$ such that the conormal-conormal moment

satisfies $\sigma^{\mathrm{nn}} := \boldsymbol{n}^T \boldsymbol{\sigma} \boldsymbol{n} = \boldsymbol{n}^T \boldsymbol{\rho} \boldsymbol{n}$ on Σ_{s}. Since the second term in (3.8) contains boundary integral portions on Σ_{c}, where $\boldsymbol{n} \cdot \nabla_\Gamma w \neq 0$, then $\boldsymbol{\sigma}$ and w satisfy a modified form of (3.10):

$$a(\boldsymbol{\sigma}, \boldsymbol{\varphi}) + b_h(\boldsymbol{\varphi}, w) = (\varphi^{\mathrm{nn}}, \boldsymbol{n} \cdot \nabla_\Gamma g)_{\Sigma_{\mathrm{c}}} \quad \forall \boldsymbol{\varphi} \in \mathcal{V}_h. \tag{3.12}$$

Moreover, writing $\boldsymbol{\sigma} = \mathring{\boldsymbol{\sigma}} + \boldsymbol{\rho}$, with $\mathring{\boldsymbol{\sigma}} \in \mathcal{V}_h$, we have

$$a(\mathring{\boldsymbol{\sigma}}, \boldsymbol{\varphi}) = -a(\boldsymbol{\rho}, \boldsymbol{\varphi}) - \mathring{b}_h(\boldsymbol{\varphi}, w) \ \ \forall \boldsymbol{\varphi} \in \mathcal{V}_h, \tag{3.13}$$

where we defined $\mathring{b}_h(\boldsymbol{\varphi}, v) := b_h(\boldsymbol{\varphi}, v) - (\varphi^{\mathrm{nn}}, \boldsymbol{n} \cdot \nabla_\Gamma v)_{\Sigma_{\mathrm{c}}}$ (i.e., it has no boundary term). Clearly, $\|\mathring{\boldsymbol{\sigma}}\|_{L^2(\Gamma)} \leq \|\boldsymbol{\rho}\|_{L^2(\Gamma)} + \|\nabla_\Gamma \nabla_\Gamma w\|_{L^2(\Gamma)}$. See subsection 4.4 for the fully discrete method.

3.5. Mapping properties. In order to analyze the error in our approximation scheme (4.9), we need a few results on how functions transform between discrete surfaces Γ^m and Γ^l for $m \neq l$, as well as how the forms $b_h^m(\cdot,\cdot)$, $a^m(\cdot,\cdot)$ and $b_h^l(\cdot,\cdot)$, $a^l(\cdot,\cdot)$ are related.

3.5.1. The Piola transform. The tangent space on Γ^m is elementwise defined through the mesh $\mathcal{T}_h^m$. We require a transformation rule that relates functions in $H_h^0(\Gamma^m; \mathbf{S}^m)$ to $H_h^0(\Gamma^l; \mathbf{S}^l)$ (with $m \neq l$) such that *conormal-conormal continuity* is preserved; this is crucial to ensure that the HHJ finite element space in (4.3) is continuous. We first recall the surface matrix Piola transform from [40, Def. 4.6].

DEFINITION 3.3. *Recall the curved element mapping discussion in subsection* 3.1. *Let* $\boldsymbol{J} = (\nabla_{T^1} \boldsymbol{F}_T^m) \bar{\boldsymbol{P}}_\star \in \mathbb{R}^{3\times 2}$, *where* ∇_{T^1} *is the surface gradient on* $T^1 \in \mathcal{T}_h^1$, $(\nabla_{T^1} \boldsymbol{F}_T^m) \in \mathbb{R}^{3\times 3}$, *and* $\bar{\boldsymbol{P}}_\star \in \mathbb{R}^{3\times 2}$ *is the projection and restriction onto the tangent space of* T^1. *Given an extrinsic tensor* $\bar{\boldsymbol{\varphi}} : \Gamma^1 \to \mathbf{S}^1$ *on the piecewise linear surface* Γ^1, *we map it (elementwise) to a tensor* $\tilde{\boldsymbol{\varphi}} : \Gamma^m \to \mathbf{S}^m$ *for any* m, *using the map* $\tilde{\mathbf{x}} = \boldsymbol{F}_T^m(\bar{\mathbf{x}})$ *and*

$$\tilde{\boldsymbol{\varphi}}(\tilde{\mathbf{x}}) = Piola(\bar{\boldsymbol{\varphi}})(\bar{\mathbf{x}}) := \det(\boldsymbol{Q})^{-1} \boldsymbol{J} \bar{\boldsymbol{P}}_\star^{\ T} \bar{\boldsymbol{\varphi}}(\bar{\mathbf{x}}) \bar{\boldsymbol{P}}_\star \boldsymbol{J}^T, \tag{3.14}$$

where $\boldsymbol{Q} = \boldsymbol{J}^T \boldsymbol{J}$. *The inverse Piola transform is given by*

$$\bar{\boldsymbol{\varphi}}(\bar{\mathbf{x}}) = Piola^{-1}(\tilde{\boldsymbol{\varphi}})(\tilde{\mathbf{x}}) := \det(\boldsymbol{Q}) \bar{\boldsymbol{P}}_\star \boldsymbol{Q}^{-1} \boldsymbol{J}^T \tilde{\boldsymbol{\varphi}}(\tilde{\mathbf{x}}) \boldsymbol{J} \boldsymbol{Q}^{-1} \bar{\boldsymbol{P}}_\star^{\ T}. \tag{3.15}$$

Remark 3.4. A tangential tensor $\hat{\boldsymbol{\varphi}}$ defined on Γ^l is mapped to a tensor $\tilde{\boldsymbol{\varphi}}$ on Γ^m, for $m \neq l$, through the map $\boldsymbol{\Phi}^{lm}$ (see (3.1)). In other words, $\hat{\boldsymbol{\varphi}}$ is mapped to $\bar{\boldsymbol{\varphi}}$ on Γ^1 using (3.15), and then $\bar{\boldsymbol{\varphi}}$ is mapped to $\tilde{\boldsymbol{\varphi}}$ on Γ^m using (3.14).

Adopting the hypothesis of Definition 3.3, we recall [40, Prop. 4.7], which states

$$\tilde{\varphi}^{\mathrm{nn}} \circ \boldsymbol{F}_T^m = \bar{\varphi}^{\mathrm{nn}} |(\nabla_{T^1} \boldsymbol{F}_T^m) \bar{\boldsymbol{t}}|^{-2}. \tag{3.16}$$

Since $\boldsymbol{F}^m$ is piecewise smooth and continuous with respect to the mesh $\mathcal{T}_h^1$, it follows that $(\nabla_{T^1} \boldsymbol{F}_T^m) \bar{\boldsymbol{t}}$ is single-valued at interelement edges, so $\tilde{\boldsymbol{\varphi}}$ is conormal-conormal continuous if and only if $\bar{\boldsymbol{\varphi}}$ is. This leads to the following norm equivalence (see [40, eq. (4.15)]):

$$\|\tilde{\boldsymbol{\varphi}}\|_{0,h,m} \approx \|\hat{\boldsymbol{\varphi}}\|_{0,h,l} \, \forall \tilde{\boldsymbol{\varphi}} \in H_h^0(\Gamma^m; \mathbf{S}^m), \ \forall \ 1 \leq l, m \leq k, \infty. \tag{3.17}$$

3.5.2. Mapping forms. The following result, which is an improved version of [40, Thm. 4.8], is essential for analyzing the geometric error between the approximate solution on an approximate domain and the exact solution on the exact domain. Recall that $\Gamma \in C^p$ with $p \geq 2$.

THEOREM 3.5. *Let $1 \le l \le p-1$ and suppose that either $l < m$, for $1 < m \le p-1$, or $m = \infty$, and recall the mapping discussion in subsection* 3.1. *Let $\tilde{\boldsymbol{\sigma}} \in H_h^0(\Gamma^m; \mathbf{S}^m)$, $\hat{\boldsymbol{\sigma}} \in H_h^0(\Gamma^l; \mathbf{S}^l)$, and $\bar{\boldsymbol{\sigma}} \in H_h^0(\Gamma^1; \mathbf{S}^1)$ and assume they are related through the Piola transform (Definition* 3.3*) in the sense of Remark* 3.4. *Make the same assumption for $\tilde{\boldsymbol{\varphi}}$, $\hat{\boldsymbol{\varphi}}$, $\bar{\boldsymbol{\varphi}}$. In addition, let $\tilde{v} \in H_h^2(\Gamma^m)$, $\hat{v} \in H_h^2(\Gamma^l)$, $\bar{v} \in H_h^2(\Gamma^1)$, where $\tilde{v}|_T \circ \boldsymbol{\Phi}_T^{1m} = \bar{v}$ and $\hat{v}|_T \circ \boldsymbol{\Phi}_T^{1l} = \bar{v}$. Then, there holds*

$$a^m(\tilde{\boldsymbol{\sigma}}, \tilde{\boldsymbol{\varphi}}) = a^l(\hat{\boldsymbol{\sigma}}, \hat{\boldsymbol{\varphi}}) + O(h^l)\|\hat{\boldsymbol{\sigma}}\|_{L^2(\Gamma^l)}\|\hat{\boldsymbol{\varphi}}\|_{L^2(\Gamma^l)}, \tag{3.18}$$

$$\begin{aligned} b_h^m(\tilde{\boldsymbol{\varphi}}, \tilde{v}) &= b_h^l(\hat{\boldsymbol{\varphi}}, \hat{v}) + O(h^l)\|\hat{\boldsymbol{\varphi}}\|_{0,h,l}\left(\|\hat{v}\|_{2,h,l} + |\hat{v}|_{H^1(\Gamma^l)}\right) \\ &\quad - b_h^1\left(\bar{\boldsymbol{\varphi}}, (\boldsymbol{F}^m - \boldsymbol{F}^l)\cdot \mathrm{P}_0 \nabla_{\Gamma^1}\bar{v}\right) \\ &\quad + \sum_{E^1 \in \mathcal{E}_{\partial,h}^1} \left\langle \bar{\varphi}^{\mathrm{nn}}, \partial_{\bar{\mathrm{s}}}\left(\boldsymbol{F}_T^m - \boldsymbol{F}_T^l\right)\cdot \mathrm{M}_0(\boldsymbol{\nu}\times\tilde{\boldsymbol{t}})\left(\bar{\boldsymbol{t}}\cdot\nabla_{T^1}\mathcal{I}_h^{1,1}\bar{v}\right)\right\rangle_{E^1}, \end{aligned} \tag{3.19}$$

where $\partial_{\bar{\mathrm{s}}}$ is the derivative with respect to arc-length on E^1, $\mathcal{I}_h^{1,1}$ is the Lagrange interpolation operator onto piecewise linears on Γ^1, P_0 is the $L^2(\Gamma^1)$ projection onto piecewise constants, M_0 maps piecewise smooth functions on $\mathcal{E}_{\partial,h}^1$ to piecewise constants via $\mathrm{M}_0 v|_{E^1} := v(m_0)$ with m_0 the midpoint of E^1, and $\boldsymbol{\nu} \equiv \boldsymbol{\nu}\circ\boldsymbol{F}_T$ is the unit normal vector of T (see Theorem 3.1*).*

Proof. We start with the result of [40, Thm. 4.8], which already proves (3.18). Furthermore, we have the following from [40, eq. (4.17)]:

$$\begin{aligned} b_h^m(\tilde{\boldsymbol{\varphi}}, \tilde{v}) &= b_h^l(\hat{\boldsymbol{\varphi}}, \hat{v}) + O(h^l)\|\hat{\boldsymbol{\varphi}}\|_{0,h,l}\left(\|\hat{v}\|_{2,h,l} + |\hat{v}|_{H^1(\Gamma^l)}\right) \\ &\quad - b_h^1\left(\bar{\boldsymbol{\varphi}}, (\boldsymbol{F}^m - \boldsymbol{F}^l)\cdot \mathrm{P}_0\nabla_{\Gamma^1}\bar{v}\right) + \sum_{E^1\in\mathcal{E}_{\partial,h}^1}\left\langle \bar{\varphi}^{\mathrm{nn}}, \beta\bar{\boldsymbol{t}}\cdot\nabla_{T^1}\mathcal{I}_h^{1,1}\bar{v}\right\rangle_{E^1}, \end{aligned} \tag{3.20}$$

where $\beta = [(\tilde{\boldsymbol{t}} - \hat{\boldsymbol{t}})\times\boldsymbol{\nu}]\cdot\tilde{\boldsymbol{t}} = (\tilde{\boldsymbol{t}} - \hat{\boldsymbol{t}})\cdot(\boldsymbol{\nu}\times\tilde{\boldsymbol{t}})$. Note that the tangent vectors are obtained from the local element map:

$$\tilde{\boldsymbol{t}} = \frac{(\nabla_{T^1}\boldsymbol{F}_T^m)\bar{\boldsymbol{t}}}{|(\nabla_{T^1}\boldsymbol{F}_T^m)\bar{\boldsymbol{t}}|}, \quad \hat{\boldsymbol{t}} = \frac{(\nabla_{T^1}\boldsymbol{F}_T^l)\bar{\boldsymbol{t}}}{|(\nabla_{T^1}\boldsymbol{F}_T^l)\bar{\boldsymbol{t}}|}, \tag{3.21}$$

where $\bar{\boldsymbol{t}}$ is the tangent vector of the straight element $E^1 \in \mathcal{E}_{\partial,h}^1$. Since $\tilde{\boldsymbol{t}}\cdot(\boldsymbol{\nu}\times\tilde{\boldsymbol{t}}) = 0$, we derive another expression for β:

$$\begin{aligned} \beta &= \left(\frac{|(\nabla_{T^1}\boldsymbol{F}_T^m)\bar{\boldsymbol{t}}|}{|(\nabla_{T^1}\boldsymbol{F}_T^l)\bar{\boldsymbol{t}}|}\tilde{\boldsymbol{t}} - \hat{\boldsymbol{t}}\right)\cdot(\boldsymbol{\nu}\times\tilde{\boldsymbol{t}}) \\ &= |(\nabla_{T^1}\boldsymbol{F}_T^l)\bar{\boldsymbol{t}}|^{-1}\left((\nabla_{T^1}\boldsymbol{F}_T^m)\bar{\boldsymbol{t}} - (\nabla_{T^1}\boldsymbol{F}_T^l)\bar{\boldsymbol{t}}\right)\cdot(\boldsymbol{\nu}\times\tilde{\boldsymbol{t}}) \\ &= \left(|(\nabla_{T^1}\boldsymbol{F}_T^l)\bar{\boldsymbol{t}}|^{-1} - 1\right)\bar{\boldsymbol{t}}^T\left(\nabla_{T^1}\left(\boldsymbol{F}_T^m - \boldsymbol{F}_T^l\right)\right)(\boldsymbol{\nu}\times\tilde{\boldsymbol{t}}) \\ &\quad + \left((\nabla_{T^1}\boldsymbol{F}_T^m)\bar{\boldsymbol{t}} - (\nabla_{T^1}\boldsymbol{F}_T^l)\bar{\boldsymbol{t}}\right)\cdot(\boldsymbol{\nu}\times\tilde{\boldsymbol{t}}) \\ &= \left((\nabla_{T^1}\boldsymbol{F}_T^m)\bar{\boldsymbol{t}} - (\nabla_{T^1}\boldsymbol{F}_T^l)\bar{\boldsymbol{t}}\right)\cdot(\boldsymbol{\nu}\times\tilde{\boldsymbol{t}}) + O(h^{l+1}), \end{aligned} \tag{3.22}$$

where we used two of the estimates in (3.2). Continuing, we find that

$$\begin{aligned} \beta &= \left((\nabla_{T^1}\boldsymbol{F}_T^m)\bar{\boldsymbol{t}} - (\nabla_{T^1}\boldsymbol{F}_T^l)\bar{\boldsymbol{t}}\right)\cdot\mathrm{M}_0(\boldsymbol{\nu}\times\tilde{\boldsymbol{t}}) \\ &\quad + \bar{\boldsymbol{t}}^T\left(\nabla_{T^1}\left(\boldsymbol{F}_T^m - \boldsymbol{F}_T^l\right)\right)\left[(\boldsymbol{\nu}\times\tilde{\boldsymbol{t}}) - \mathrm{M}_0(\boldsymbol{\nu}\times\tilde{\boldsymbol{t}})\right] + O(h^{l+1}), \\ &= \left((\nabla_{T^1}\boldsymbol{F}_T^m)\bar{\boldsymbol{t}} - (\nabla_{T^1}\boldsymbol{F}_T^l)\bar{\boldsymbol{t}}\right)\cdot\mathrm{M}_0(\boldsymbol{\nu}\times\tilde{\boldsymbol{t}}) + O(h^{l+1}), \end{aligned} \tag{3.23}$$

where we used the second estimate in (3.2) and $\mathrm{M}_0(\boldsymbol{\nu}\times\tilde{\boldsymbol{t}})$ is the midpoint evaluation. Note that $\|(\boldsymbol{\nu}\times\tilde{\boldsymbol{t}})-\mathrm{M}_0(\boldsymbol{\nu}\times\tilde{\boldsymbol{t}})\|_{L^\infty(E^1)}\leq Ch$, which follows by a simple Taylor expansion where the constant C depends on the curvature of Γ and Σ.

Next, note that $(\nabla_{T^1}\boldsymbol{F}_T^m)\bar{\boldsymbol{t}}-(\nabla_{T^1}\boldsymbol{F}_T^l)\bar{\boldsymbol{t}}=\partial_{\bar{\mathrm{s}}}(\boldsymbol{F}_T^m-\boldsymbol{F}_T^l)$, where $\partial_{\bar{\mathrm{s}}}$ is the derivative with respect to arc-length on E^1. Thus, we get

$$\begin{aligned}&\sum_{E^1\in\mathcal{E}^1_{\partial,h}}\left\langle\bar{\varphi}^{\mathrm{nn}},\beta\bar{\boldsymbol{t}}\cdot\nabla_{T^1}\mathcal{I}_h^{1,1}\bar{v}\right\rangle_{E^1}\\&\qquad\leq\sum_{E^1\in\mathcal{E}^1_{\partial,h}}\left\langle\bar{\varphi}^{\mathrm{nn}},\partial_{\bar{\mathrm{s}}}\left(\boldsymbol{F}_T^m-\boldsymbol{F}_T^l\right)\cdot\boldsymbol{C}_{E^1}\right\rangle_{E^1}+O(h^l)\|\hat{\boldsymbol{\varphi}}\|_{0,h,l}|\hat{v}|_{H^1(\Gamma^l)},\end{aligned}\tag{3.24}$$

where $\boldsymbol{C}_{E^1}:=\mathrm{P}_0(\boldsymbol{\nu}\times\tilde{\boldsymbol{t}})(\bar{\boldsymbol{t}}\cdot\nabla_{T^1}\mathcal{I}_h^{1,1}\bar{v})$ is defined on $E^1\in\mathcal{E}^1_{\partial,h}$, and we used equivalence of norms. The result (3.19) then follows. ∎

A simple consequence of Theorem 3.5 is

$$b_h^m(\boldsymbol{\varphi},v)=b_h^l(\hat{\boldsymbol{\varphi}},\hat{v})+O(h^{l-1})\|\hat{\boldsymbol{\varphi}}\|_{0,h,l}\|\hat{v}\|_{2,h,l}.\tag{3.25}$$

4. Finite element approximation. In defining the polynomial degree of the finite element spaces, we utilize the integer $r\geq 0$. The polynomial degree of each space cannot be chosen independently. Specifically, the (surface) Lagrange finite element space is degree $r+1$ and the (surface) HHJ space is degree r. This is necessary to ensure various compatibility conditions [3, 40], such as (4.6).

4.1. Curved Lagrange spaces. Let $m\geq 1$ be an integer or ∞. The (continuous) Lagrange finite element space of degree $r+1$ is defined on Γ^m by the mapping $\boldsymbol{F}_T^m$:

$$W_h^{m,r+1}\equiv W_h^{m,r+1}(\Gamma^m):=\{v\in H_h^2(\Gamma^m)\mid v|_T\circ\boldsymbol{F}_T^m\in\mathcal{P}_{r+1}(T^1)\;\forall T\in\mathcal{T}_h^m\},\tag{4.1}$$

where we will sometimes suppress the $r+1$ superscript, i.e., we make the abbreviation $W_h^{m,r+1}\equiv W_h^m$. For the case $m=\infty$ (the exact domain) we simply write W_h.

Again, owing to the continuous embedding $H_h^2(\Gamma^1)\hookrightarrow C^0(\overline{\Gamma^1})$ (see [41, Thm. 4.2]), we can define the Lagrange interpolation operator $\mathcal{I}_h^1:H_h^2(\Gamma^1)\to W_h^1$ [5], defined on each element $T^1\in\mathcal{T}_h^1$ by

$$(\mathcal{I}_h^1v)(\mathbf{x})-v(\mathbf{x})=0,\quad\int_{E^1}(\mathcal{I}_h^1v-v)q\,d\mathrm{s}=0,\quad\int_{T^1}(\mathcal{I}_h^1v-v)\eta\,d\mathrm{S}=0\tag{4.2}$$

for all vertices $\mathbf{x}$ of T^1, all $q\in\mathcal{P}_{r-1}(E^1)$ (and all $E^1\in\partial T^1$), and all $\eta\in\mathcal{P}_{r-2}(T^1)$. Note that when $r=0$, the last two conditions in (4.2) are omitted. When $r=1$, the second condition is enforced by constant functions q on E^1 and the last condition is omitted. When $r\geq 2$, all conditions in (4.2) are present.

Then, given $v\in H_h^2(\Gamma^m)$, we define the global interpolation operator, $\mathcal{I}_h^m:H_h^2(\Gamma^m)\to W_h^m$, elementwise through $\mathcal{I}_h^mv\big|_{T^m}\circ\boldsymbol{F}_T^m:=\mathcal{I}_h^1(v\circ\boldsymbol{F}_T^m)$. The approximation properties of $\mathcal{I}_h^m$ are standard. We also denote $\mathcal{I}_h^{m,s}$ to be the above Lagrange interpolant on Γ^m onto continuous piecewise polynomials of degree s, and we make the following abbreviation $\mathcal{I}_h^{m,r+1}\equiv\mathcal{I}_h^m$.

4.2. The HHJ finite element space. We give a brief overview of the surface HHJ space; see [40, sect. 5.2] for more details. On the piecewise linear surface triangulation Γ^1, we start with a space of (piecewise) tangential, tensor-valued functions with special continuity properties. Let

$$\mathcal{M}_{\mathrm{nn}}^1(\Gamma^1):=\{\boldsymbol{\varphi}\in L^2(\Gamma^1;\mathbf{S}^1)\mid\boldsymbol{\varphi}|_{T^1}\in H^1(T^1;\mathbf{S}^1)\;\forall T^1\in\mathcal{T}_h^1,\text{ with }\boldsymbol{\varphi}\text{ cn-cn contin.}\},$$

where "cn-cn contin." means the *conormal-conormal continuity* condition that holds at interelement boundaries, i.e., for any pair of triangles (T_a^1, T_b^1) in $\mathcal{T}_h^1$ that share an edge $E^1 = \overline{T_a^1} \cap \overline{T_b^1}$, we have $\boldsymbol{n}_a^T \boldsymbol{\varphi} \boldsymbol{n}_a|_{E^1} = \boldsymbol{n}_b^T \boldsymbol{\varphi} \boldsymbol{n}_b|_{E^1}$, where $\boldsymbol{n}_a$ ($\boldsymbol{n}_b$) is the outer conormal of ∂T_a^1 (∂T_b^1); note that, in general, $\boldsymbol{n}_a \neq -\boldsymbol{n}_b$ (on E^1).

Remark 4.1. The surface normal $\boldsymbol{\nu}^1$ of Γ^1 is discontinuous at edges of triangles in Γ^1, thus the space of tangential tensors $\mathbf{S}^1$ is not well-defined at edges of Γ^1. Thus, we define $\mathbf{S}^1(T^1) := \{\boldsymbol{\varphi} : T^1 \to \mathbb{R}^{3\times 3} \mid \boldsymbol{\varphi} = \boldsymbol{\varphi}^T,\ \boldsymbol{\varphi}\boldsymbol{\nu}^1 = \mathbf{0}\}$ for all $T^1 \in \mathcal{T}_h^1$, and then $\mathbf{S}^1 \equiv \mathbf{S}^1(\Gamma^1) := \{\boldsymbol{\varphi} : \Gamma^1 \to \mathbb{R}^{3\times 3} \mid \boldsymbol{\varphi}|_{T^1} \in \mathbf{S}^1(T^1)\ \forall T^1 \in \mathcal{T}_h^1\}$. Therefore, $L^2(\Gamma^1; \mathbf{S}^1) := \{\boldsymbol{\varphi} \in L^2(\Gamma^1; \mathbb{R}^{3\times 3}) \,|\, \boldsymbol{\varphi}|_{T^1} \in L^2(T^1; \mathbf{S}^1(T^1))\ \forall T^1 \in \mathcal{T}_h^1\}$.

Clearly, $\mathcal{M}_{\mathrm{nn}}^1(\Gamma^1) \subset H_h^0(\Gamma^1; \mathbf{S}^1)$. For $1 \leq m \leq k, \infty$, where $\Gamma^\infty \equiv \Gamma$, we also have the space

$$\mathcal{M}_{\mathrm{nn}}^m(\Gamma^m) := \{\boldsymbol{\varphi} \in L^2(\Gamma^m; \mathbf{S}^m) \,|\, \boldsymbol{\varphi} \circ \boldsymbol{F}^m := \mathrm{Piola}(\bar{\boldsymbol{\varphi}}),\ \bar{\boldsymbol{\varphi}} \in \mathcal{M}_{\mathrm{nn}}^1(\Gamma^1)\},$$

where the Piola transform is defined elementwise, using $\boldsymbol{F}^m$; by (3.16), $\mathcal{M}_{\mathrm{nn}}^m(\Gamma^m)$ also satisfies the conormal-conormal continuity property. Note that $L^2(\Gamma^m; \mathbf{S}^m)$ is defined similarly to $L^2(\Gamma^1; \mathbf{S}^1)$ in Remark 4.1.

The conforming, HHJ finite element space on Γ^1, of degree $r \geq 0$, is defined by $V_h^{1,r} := \{\boldsymbol{\varphi} \in \mathcal{M}_{\mathrm{nn}}^1(\Gamma^1) \,|\, \boldsymbol{\varphi}|_{T^1} \in \mathcal{P}_r(T^1; \mathbf{S}^1)\ \forall T^1 \in \mathcal{T}_h^1\}$. Using the Piola transform, for $1 \leq m \leq k, \infty$, we also have

$$V_h^{m,r} := \{\boldsymbol{\varphi} \in \mathcal{M}_{\mathrm{nn}}^m(\Gamma^m) \,|\, \boldsymbol{\varphi} \circ \boldsymbol{F}^m := \mathrm{Piola}(\bar{\boldsymbol{\varphi}}),\ \bar{\boldsymbol{\varphi}} \in V_h^{1,r}\}, \tag{4.3}$$

where we will sometimes suppress the r superscript, i.e., we make the abbreviation $V_h^{m,r} \equiv V_h^m$. For the case $m = \infty$ (the exact domain) we simply write V_h. We note the following norm equivalence in [40, eq. (5.5)]:

$$\|\boldsymbol{\varphi}\|_{0,h,m} \approx \|\boldsymbol{\varphi}\|_{L^2(\Gamma^m)}\ \forall\, \boldsymbol{\varphi} \in V_h^m. \tag{4.4}$$

There exists an interpolation operator $\Pi_h^m : \mathcal{M}_{\mathrm{nn}}^m(\Gamma^m) \to V_h^m$, defined elementwise, that satisfies many basic approximation results which can be found in [3, Supp. Mater.], [40, sect. 5.2]. For simplicity, we describe the operator on Γ^1 only, i.e., $\Pi_h^1 : \mathcal{M}_{\mathrm{nn}}^1(\Gamma^1) \to V_h^1$ [10, 5] is defined on each element $T^1 \in \mathcal{T}_h^1$ by

$$\int_{E^1} \boldsymbol{n}^T \left[\Pi_h^1 \boldsymbol{\varphi} - \boldsymbol{\varphi}\right] \boldsymbol{n}\, q\, d\mathrm{s} = 0, \quad \int_{T^1} \left[\Pi_h^1 \boldsymbol{\varphi} - \boldsymbol{\varphi}\right] : \boldsymbol{\eta}\, d\mathrm{S} = 0 \tag{4.5}$$

for all $q \in \mathcal{P}_r(E^1)$ (and all $E^1 \in \partial T^1$) and all $\boldsymbol{\eta} \in \mathcal{P}_{r-1}(T^1; \mathbf{S})$. We note that the degrees-of-freedom for V_h^1 are given by (4.5), [10, Lem. 3], [28]. On affine elements, we have a Fortin-like property involving $b_h^1(\cdot,\cdot)$ for any degree $r \geq 0$ [10, 5, 8]:

$$\begin{aligned}
b_h^1\left(\boldsymbol{\varphi} - \Pi_h^1 \boldsymbol{\varphi}, \theta_h v_h\right) &= 0 \quad \forall \boldsymbol{\varphi} \in H_h^0(\Gamma^1; \mathbf{S}^1), \quad v_h \in W_h^1, \\
b_h^1\left(\boldsymbol{\varphi}_h, (v - \mathcal{I}_h^1 v)\theta_h\right) &= 0 \quad \forall \boldsymbol{\varphi}_h \in V_h^1, \quad v \in H_h^2(\Gamma^1), \\
\left(\varphi_h^{\mathrm{nn}}, \partial_{\mathrm{s}}\left(v - \mathcal{I}_h^1 v\right)\eta_h\right)_{\mathcal{E}_{\partial,h}^1} &= 0 \quad \forall \boldsymbol{\varphi}_h \in V_h^1, \quad v \in H_h^2(\Gamma^1),
\end{aligned} \tag{4.6}$$

where the degree of $W_h^1 \equiv W_h^{1,r+1}$ is $r+1$ and the degree of $V_h^1 \equiv V_h^{1,r}$ is r. The orthogonality property in (4.6) holds for *any* piecewise constant functions θ_h (η_h) defined on $\mathcal{T}_h^1$ ($\mathcal{E}_{\partial,h}^1$); the first two properties are noted in [10, 5, 8].

4.3. The HHJ projection. We pose (3.10) on Γ^m with continuous skeleton spaces denoted $\mathcal{V}_h^m \equiv \mathcal{V}_h(\Gamma^m)$ and $\mathcal{W}_h^m \equiv \mathcal{W}_h(\Gamma^m)$. Fixing the polynomial degree $r \geq 0$, the conforming finite element spaces are $V_h^m \subset \mathcal{V}_h^m$, $W_h^m \subset \mathcal{W}_h^m$, where we abuse notation by now *enforcing essential boundary conditions* directly in the definitions of V_h^m and W_h^m. The finite element approximation to (3.10) is as follows. Given any $\hat{w}_h \in \mathcal{W}_h^m$, find $\hat{\boldsymbol{\sigma}}_h \in V_h^m$ such that

$$a^m\left(\hat{\boldsymbol{\sigma}}_h, \hat{\boldsymbol{\varphi}}_h\right) + b_h^m\left(\hat{\boldsymbol{\varphi}}_h, \hat{w}_h\right) = 0 \quad \forall\, \hat{\boldsymbol{\varphi}}_h \in V_h^m. \tag{4.7}$$

Note that when $m = 1$, $r = 0$, Hessian information is captured by the jump terms in $b_h^m\left(\hat{\boldsymbol{\varphi}}_h, \hat{w}_h\right)$. Since $a^m(\cdot,\cdot)$ is continuous and coercive over V_h^m, by (4.4), we get

$$\begin{aligned} \|\hat{\boldsymbol{\sigma}}_h\|_{L^2(\Gamma^m)}^2 = a^m\left(\hat{\boldsymbol{\sigma}}_h, \hat{\boldsymbol{\sigma}}_h\right) = -b_h^m\left(\hat{\boldsymbol{\sigma}}_h, w_h\right) &\leq \|\hat{\boldsymbol{\sigma}}_h\|_{0,h,m}\|\hat{w}_h\|_{2,h,m} \\ &\leq C\|\hat{\boldsymbol{\sigma}}_h\|_{L^2(\Gamma^m)}\|\hat{w}_h\|_{2,h,m} \end{aligned} \tag{4.8}$$

for some independent constant $C > 0$. Thus, $\hat{\boldsymbol{\sigma}}_h$ is a stable $L^2(\Gamma^m)$ projection. In a sense, $\hat{\boldsymbol{\sigma}}_h$ can be viewed as a discrete Hessian of $\hat{w}_h$ (see the error estimate in (4.22)).

4.4. Inhomogeneous boundary conditions. We modify (4.7) to incorporate nonzero boundary conditions, i.e., we give a discrete version of (3.12). For any $w \in H^{r+3}(\Gamma)$, we define $\tilde{w} := w \circ \boldsymbol{\Psi}^m \in H_h^2(\Gamma^m)$ and set $\tilde{\boldsymbol{\xi}} := (\nabla_\Gamma w) \circ \boldsymbol{\Psi}^m$. Then, we seek $\hat{\boldsymbol{\sigma}}_h = \mathring{\hat{\boldsymbol{\sigma}}}_h + \hat{\boldsymbol{\rho}}_h$, with $\mathring{\hat{\boldsymbol{\sigma}}}_h \in V_h^m$, such that

$$a^m\left(\mathring{\hat{\boldsymbol{\sigma}}}_h, \hat{\boldsymbol{\varphi}}_h\right) = -a^m\left(\hat{\boldsymbol{\rho}}_h, \hat{\boldsymbol{\varphi}}_h\right) - b_h^m\left(\hat{\boldsymbol{\varphi}}_h, \tilde{w}\right) + \left(\hat{\varphi}_h^{\mathrm{nn}}, \hat{\boldsymbol{n}} \cdot \tilde{\boldsymbol{\xi}}\right)_{\Sigma_c^m} \quad \forall \hat{\boldsymbol{\varphi}}_h \in V_h^m, \tag{4.9}$$

where $\hat{\boldsymbol{\rho}}_h := \mathrm{B}_h^m \tilde{\boldsymbol{\rho}}$, with $\tilde{\boldsymbol{\rho}}$ satisfying $\boldsymbol{\rho} \circ \boldsymbol{\Psi}^m = \tilde{\boldsymbol{\rho}}$, and $\mathrm{B}_h^m : H_h^0(\Gamma^m) \to V_h^m$ is the projection on Γ^m, i.e.,

$$\left(\hat{\boldsymbol{\rho}}_h - \widetilde{\boldsymbol{\rho}}, \hat{\boldsymbol{\varphi}}_h\right)_{\mathcal{T}_h^m} + \left(\hat{\boldsymbol{n}}^T[\hat{\boldsymbol{\rho}}_h - \widetilde{\boldsymbol{\rho}}]\hat{\boldsymbol{n}}, \hat{\varphi}_h^{\mathrm{nn}}\right)_{\mathcal{E}_h^m} = 0 \;\forall\, \hat{\boldsymbol{\varphi}}_h \in V_h^m, \tag{4.10}$$

which satisfies the approximation property $\|\hat{\boldsymbol{\rho}}_h - \widetilde{\boldsymbol{\rho}}\|_{0,h,m} \leq C h^{\min(r+1,m)} \|\boldsymbol{\rho}\|_{H^{r+1}(\Gamma)}$.

Choosing $\hat{\boldsymbol{\varphi}}_h = \mathring{\hat{\boldsymbol{\sigma}}}_h$ in (4.9), we have

$$\begin{aligned} \|\mathring{\hat{\boldsymbol{\sigma}}}_h\|_{L^2(\Gamma^m)}^2 &= -a^m\left(\hat{\boldsymbol{\rho}}_h, \mathring{\hat{\boldsymbol{\sigma}}}_h\right) - \mathring{b}_h^m\left(\mathring{\hat{\boldsymbol{\sigma}}}_h, \tilde{w}\right) - \left(\hat{\boldsymbol{n}}^T \mathring{\hat{\boldsymbol{\sigma}}}_h \hat{\boldsymbol{n}}, \hat{\boldsymbol{n}} \cdot \left[\nabla_{\Gamma^m}\tilde{w} - \tilde{\boldsymbol{\xi}}\right]\right)_{\Sigma_c^m} \\ &\leq \|\hat{\boldsymbol{\rho}}_h\|_{L^2(\Gamma^m)}\|\mathring{\hat{\boldsymbol{\sigma}}}_h\|_{L^2(\Gamma^m)} + \|\mathring{\hat{\boldsymbol{\sigma}}}_h\|_{0,h,m}\|\tilde{w}\|_{2,h,m} + C\|\mathring{\hat{\boldsymbol{\sigma}}}_h\|_{L^2(\Gamma^m)}\|w\|_{H^2(\Gamma)}, \end{aligned} \tag{4.11}$$

where, since $\mathrm{id}_{\Gamma^m}^k = \mathcal{I}_h^m \mathrm{id}_\Gamma^k$, applying straightforward change of variables, standard interpolation estimates, and an inverse estimate gives (see [40])

$$\begin{aligned} \left|\left(\hat{\boldsymbol{n}}^T \mathring{\hat{\boldsymbol{\sigma}}}_h \hat{\boldsymbol{n}}, \hat{\boldsymbol{n}} \cdot \left[\nabla_{\Gamma^m}\tilde{w} - \tilde{\boldsymbol{\xi}}\right]\right)_{\Sigma_c^m}\right| &\leq O(h^{1/2})\|\mathring{\hat{\boldsymbol{\sigma}}}_h\|_{L^2(\Sigma^m)}\|w\|_{H^2(\Gamma)} \\ &\leq C\|\mathring{\hat{\boldsymbol{\sigma}}}_h\|_{L^2(\Gamma^m)}\|w\|_{H^2(\Gamma)}. \end{aligned} \tag{4.12}$$

By equivalence of norms, $\|\tilde{w}\|_{2,h,m} \approx \|w\|_{2,h} \equiv \|\nabla_\Gamma \nabla_\Gamma w\|_{L^2(\Gamma)}$ and $\|\mathring{\hat{\boldsymbol{\sigma}}}_h\|_{L^2(\Gamma^m)} \approx \|\mathring{\hat{\boldsymbol{\sigma}}}_h\|_{0,h,m}$, we obtain

$$\|\mathring{\hat{\boldsymbol{\sigma}}}_h\|_{0,h,m} \leq C\left(\|\hat{\boldsymbol{\rho}}_h\|_{L^2(\Gamma^m)} + \|w\|_{H^2(\Gamma)}\right) \tag{4.13}$$

for some constant $C > 0$ that does not depend on h. Thus, the projection is stable.

4.5. Error analysis. The stability of the surface HHJ method, as well as its convergence, depends crucially on the following choice of surface approximation. If $\Gamma \in C^p$, with $p \geq 2$, let $\widehat{\boldsymbol{F}_T^m} : T^1 \to T^m$, for all $T^1 \in \mathcal{T}_h^1$ and $1 \leq m \leq p-1$, be given by

$$\boldsymbol{F}_T^m \equiv \widehat{\boldsymbol{F}_T^m} := \mathcal{I}_h^{1,m} \boldsymbol{F}_T \equiv \mathcal{I}_h^{1,m} \boldsymbol{\Psi}_T^1, \tag{4.14}$$

where $\mathcal{I}_h^{1,m}$ is the Lagrange interpolation operator in (4.2) onto degree m polynomials; we simplify the notation by writing $\boldsymbol{F}_T^m \equiv \widehat{\boldsymbol{F}_T^m}$. This choice is *necessary* to guarantee optimal convergence of the HHJ method when $m = r+1$. If one chooses the geometric degree m to be higher than the degree of the Lagrange space $r+1$ (i.e., $m > r+1$), then $\boldsymbol{F}_T^m$ can be chosen to be the standard nodal Lagrange interpolant of $\boldsymbol{F}_T$ and preserve optimal convergence of the scheme in (4.9) (and (5.11)).

Remark 4.2. According to (4.2), if $m = 1$ (piecewise linear) the condition (4.14) means that the vertices of the discrete surface lie on the exact surface. If $m = 2$ (piecewise quadratic), then the corner vertices of the triangles must lie on the exact surface, while the edge nodes are determined through the second condition in (4.2) (i.e., the average value of $\boldsymbol{F}_T^m$ over each edge of the mesh must equal the average value of $\boldsymbol{F}_T$ over each corresponding edge), and so on for higher m. Computing these moments is straightforward since they are local problems.

For the convergence analysis, we assume $w \in H^{r+3}(\Gamma)$, where $r \geq 0$ is the degree of the HHJ space. Let $\boldsymbol{\sigma} := \nabla_\Gamma \nabla_\Gamma w \in H^{r+1}(\Gamma; \mathbf{S})$, and note that $\boldsymbol{\sigma}$ satisfies (3.12), where $\boldsymbol{\rho} \in H^{r+1}(\Gamma; \mathbf{S})$ is such that $\boldsymbol{n}^T \boldsymbol{\sigma} \boldsymbol{n} = \boldsymbol{n}^T \boldsymbol{\rho} \boldsymbol{n}$ on Σ_{s}. Next, we introduce an intermediate discrete (finite dimensional) problem posed on the exact surface. Let $\boldsymbol{\rho}_h$ be the $L^2(\Gamma)$ projection of $\boldsymbol{\rho}$ onto V_h, i.e., $\boldsymbol{\rho}_h \in V_h$ satisfies $a(\boldsymbol{\rho}_h, \boldsymbol{\varphi}_h) = a(\boldsymbol{\rho}, \boldsymbol{\varphi}_h)$ for all $\boldsymbol{\varphi}_h \in V_h$. Then, we write $\boldsymbol{\sigma}_h = \mathring{\boldsymbol{\sigma}}_h + \boldsymbol{\rho}_h$, where $\mathring{\boldsymbol{\sigma}}_h \in V_h$ satisfies

$$a(\mathring{\boldsymbol{\sigma}}_h, \boldsymbol{\varphi}_h) = -a(\boldsymbol{\rho}, \boldsymbol{\varphi}_h) - b_h(\boldsymbol{\varphi}_h, w) + (\varphi_h^{\mathrm{nn}}, \boldsymbol{n} \cdot \nabla_\Gamma w)_{\Sigma_{\mathrm{c}}} \ \forall \boldsymbol{\varphi}_h \in V_h, \tag{4.15}$$

where $\mathring{\boldsymbol{\sigma}}_h$ can be viewed as a stable projection. Comparing (4.15) with (3.13), by standard finite element analysis, utilizing Galerkin orthogonality and interpolation estimates, we have that $\|\mathring{\boldsymbol{\sigma}} - \mathring{\boldsymbol{\sigma}}_h\|_{L^2(\Gamma)} \leq \|\mathring{\boldsymbol{\sigma}} - \Pi_h \mathring{\boldsymbol{\sigma}}\|_{L^2(\Gamma)} = O(h^{r+1})$, which implies

$$\|\boldsymbol{\sigma} - \boldsymbol{\sigma}_h\|_{L^2(\Gamma)} \leq O(h^{r+1}). \tag{4.16}$$

Next, let $\hat{\boldsymbol{\sigma}}_h$ solve (4.9). To facilitate estimating the error between $\hat{\boldsymbol{\sigma}}_h$ and the exact surface Hessian $\boldsymbol{\sigma}$, we map $\boldsymbol{\sigma}_h$ to the discrete surface Γ^m, i.e., by letting $\mathring{\tilde{\boldsymbol{\sigma}}}_h \in V_h^m$ satisfy $\mathring{\boldsymbol{\sigma}}_h \circ \boldsymbol{\Psi}^m = \mathrm{Piola}(\mathring{\tilde{\boldsymbol{\sigma}}}_h)$ (recall (3.14)), and then compare $\mathring{\tilde{\boldsymbol{\sigma}}}_h$ to $\mathring{\hat{\boldsymbol{\sigma}}}_h$.

So, we apply the results of Theorem 3.5 to (4.15) to find that $\mathring{\tilde{\boldsymbol{\sigma}}}_h \in V_h^m$ satisfies

$$\begin{aligned} a^m\left(\mathring{\tilde{\boldsymbol{\sigma}}}_h, \hat{\boldsymbol{\varphi}}_h\right) &= -a^m(\tilde{\boldsymbol{\rho}}, \hat{\boldsymbol{\varphi}}_h) - b_h^m(\hat{\boldsymbol{\varphi}}_h, \tilde{w}) + \left(\hat{\varphi}_h^{\mathrm{nn}}, \hat{\boldsymbol{n}} \cdot \tilde{\boldsymbol{\xi}}\right)_{\Sigma_{\mathrm{c}}^m} \\ &\quad + O(h^m)\left(\|\mathring{\tilde{\boldsymbol{\sigma}}}_h\|_{L^2(\Gamma^m)} + \|\tilde{\boldsymbol{\rho}}\|_{L^2(\Gamma^m)}\right)\|\hat{\boldsymbol{\varphi}}_h\|_{L^2(\Gamma^m)} \\ &\quad + O(h^m)\|\hat{\boldsymbol{\varphi}}_h\|_{0,h,m}\left(\|\tilde{w}\|_{2,h,m} + |\tilde{w}|_{H^1(\Gamma^m)}\right) \\ &\quad - b_h^1(\bar{\boldsymbol{\varphi}}_h, (\boldsymbol{F} - \boldsymbol{F}^m) \cdot \mathrm{P}_0 \nabla_{\Gamma^1} \bar{w}_h) + \langle \bar{\varphi}_h^{\mathrm{nn}}, \partial_{\bar{\mathrm{s}}}(\boldsymbol{F}_T - \boldsymbol{F}_T^m) \cdot \boldsymbol{C}_{E^1} \rangle_{\mathcal{E}_{\partial,h}^1}, \end{aligned} \tag{4.17}$$

for all $\hat{\boldsymbol{\varphi}}_h$ in V_h^m, where $\boldsymbol{C}_{E^1}$ is a constant vector for each $E^1 \in \mathcal{E}_{\partial,h}^1$. We also used that

$$\left|(\varphi_h^{\mathrm{nn}}, \boldsymbol{n} \cdot \nabla_\Gamma w)_E - \left(\hat{\varphi}_h^{\mathrm{nn}}, \hat{\boldsymbol{n}} \cdot \tilde{\boldsymbol{\xi}}\right)_{E^m}\right| \leq O(h^m)\|\hat{\boldsymbol{\varphi}}_h\|_{0,h,m}\left(\|\tilde{w}\|_{2,h,m} + |\tilde{w}|_{H^1(\Gamma^m)}\right), \tag{4.18}$$

for all $E \in \mathcal{E}_{\partial,h}$ where $E^m = E \circ \boldsymbol{\Psi}^m$. Next, we make note of the assumption on $\boldsymbol{F}^m$ (4.14), use (4.6), and take advantage of equivalent norms to obtain

$$a^m\left(\mathring{\tilde{\boldsymbol{\sigma}}}_h, \hat{\boldsymbol{\varphi}}_h\right) = -a^m\left(\tilde{\boldsymbol{\rho}}, \hat{\boldsymbol{\varphi}}_h\right) - b_h^m\left(\hat{\boldsymbol{\varphi}}_h, \tilde{w}\right) + \left(\hat{\varphi}_h^{\mathrm{nn}}, \hat{\boldsymbol{n}} \cdot \tilde{\boldsymbol{\xi}}\right)_{\Sigma_c^m} + O(h^m)\|\hat{\boldsymbol{\varphi}}_h\|_{L^2(\Gamma^m)}\left(\|\boldsymbol{\rho}\|_{L^2(\Gamma)} + \|w\|_{H^2(\Gamma)}\right) \quad \forall\, \hat{\boldsymbol{\varphi}}_h \in V_h^m, \tag{4.19}$$

where we also note that $C\|\mathring{\tilde{\boldsymbol{\sigma}}}_h\|_{L^2(\Gamma^m)} \le \|\mathring{\boldsymbol{\sigma}}_h\|_{L^2(\Gamma)} \le \|\boldsymbol{\rho}\|_{L^2(\Gamma)} + \|\nabla_\Gamma \nabla_\Gamma w\|_{L^2(\Gamma)}$, for some independent constant $C > 0$. Comparing (4.19) against (4.9), we get

$$\begin{aligned} a^m\left(\mathring{\tilde{\boldsymbol{\sigma}}}_h - \mathring{\hat{\boldsymbol{\sigma}}}_h, \hat{\boldsymbol{\varphi}}_h\right) &= a^m\left(\hat{\boldsymbol{\rho}}_h - \tilde{\boldsymbol{\rho}}, \hat{\boldsymbol{\varphi}}_h\right) + O(h^m)\|\hat{\boldsymbol{\varphi}}_h\|_{L^2(\Gamma^m)}\left(\|\boldsymbol{\rho}\|_{L^2(\Gamma)} + \|w\|_{H^2(\Gamma)}\right) \\ &\le \|\hat{\boldsymbol{\varphi}}_h\|_{L^2(\Gamma^m)}\left[O(h^{r+1})\|\boldsymbol{\rho}\|_{H^{r+1}(\Gamma)} + O(h^m)\left(\|\boldsymbol{\rho}\|_{L^2(\Gamma)} + \|w\|_{H^2(\Gamma)}\right)\right] \end{aligned} \tag{4.20}$$

for all $\hat{\boldsymbol{\varphi}}_h$ in V_h^m. Therefore, we get $\|\mathring{\tilde{\boldsymbol{\sigma}}}_h - \mathring{\hat{\boldsymbol{\sigma}}}_h\|_{L^2(\Gamma^m)} \le Ch^{\min(r+1,m)}$, where the constant C depends on the $H^{r+3}(\Gamma)$ norm of Γ. Thus, we obtain

$$\|\tilde{\boldsymbol{\sigma}}_h - \hat{\boldsymbol{\sigma}}_h\|_{L^2(\Gamma^m)} \le Ch^{\min(r+1,m)}. \tag{4.21}$$

Combining the above results yields the following theorem. Note that Γ must be at least C^t if $w \in H^t(\Gamma)$ (for $t \ge 1$) because surface derivatives of w invoke corresponding derivatives of the surface parametrization.

THEOREM 4.3. *Suppose $\Gamma \in C^p$ with $p \ge 3$. Assume $r \ge 0$ is an integer such that $r+3 \le p$, let $w \in H^{r+3}(\Gamma)$, and set $\boldsymbol{\sigma} := \nabla_\Gamma \nabla_\Gamma w \in \mathbf{S}$. Furthermore, assume r is the degree of V_h^m, and let $\hat{\boldsymbol{\sigma}}_h = \mathring{\hat{\boldsymbol{\sigma}}}_h + \hat{\boldsymbol{\rho}}_h$, with $\mathring{\hat{\boldsymbol{\sigma}}}_h \in V_h^m$ satisfying (4.9) and $\hat{\boldsymbol{\rho}}_h$ defined through (4.10). If $p - 1 \ge m \ge r + 1$, then*

$$\|\boldsymbol{\sigma} - \hat{\boldsymbol{\sigma}}_h \circ (\boldsymbol{\Psi}^m)^{-1}\|_{0,h} \le Ch^{r+1}, \tag{4.22}$$

where $C > 0$ depends on the domain Γ and the shape regularity of the mesh.

Proof. Let $\boldsymbol{\sigma}_h$ be the discrete solution (defined on the exact surface) computed through (4.15), and let $\tilde{\boldsymbol{\sigma}}_h \in V_h^m$ satisfy $\boldsymbol{\sigma}_h \circ \boldsymbol{\Psi}^m = \mathrm{Piola}(\tilde{\boldsymbol{\sigma}}_h)$. It is straightforward to derive the estimate $\|\boldsymbol{\sigma}_h - \tilde{\boldsymbol{\sigma}}_h \circ (\boldsymbol{\Psi}^m)^{-1}\|_{0,h} \le O(h^{r+1})\|\tilde{\boldsymbol{\sigma}}_h\|_{0,h,m}$ (see [40, Thm. 6.4]). Then, combining with (4.16) and (4.21) through the triangle inequality, we obtain (4.22). ∎

Remark 4.4. The "exact" data $\tilde{w}$ and $\tilde{\boldsymbol{\xi}}$ can be replaced by their interpolants, $\mathcal{I}_h^m \tilde{w}$ and $\mathcal{I}_h^m \tilde{\boldsymbol{\xi}}$, without affecting the stability or accuracy of the scheme in (4.9).

In a sense, our scheme is a kind of Hessian recovery of the given discrete data $\mathcal{I}_h^m \tilde{w}$, including boundary data $\mathcal{I}_h^m \tilde{\boldsymbol{\xi}}$ and $\hat{\boldsymbol{\rho}}_h$. We note that another method of Hessian recovery for the HHJ element, developed for flat domains, is given in [29].

5. Approximating the shape operator.

Recall that, for any C^2 surface Γ, we have the identity map $\mathrm{id}_\Gamma : \Gamma \to \Gamma$ given by $\mathbf{x} = \mathrm{id}_\Gamma(\mathbf{x})$ for all $\mathbf{x} \in \Gamma$, and $\nabla_\Gamma \mathrm{id}_\Gamma = \boldsymbol{P}$ (tangent space projection). In addition, we have the shape operator $\nabla_\Gamma \boldsymbol{\nu}$ that satisfies (SM2.4): $\nabla_\Gamma \boldsymbol{\nu} = \kappa^1 \boldsymbol{d}_1 \otimes \boldsymbol{d}_1 + \kappa^2 \boldsymbol{d}_2 \otimes \boldsymbol{d}_2$, where κ^1, κ^2 are the *principle curvatures* of Γ, with $\kappa^1 \ge \kappa^2$, and $\boldsymbol{d}_1$, $\boldsymbol{d}_2$ are the *principle directions* (which are tangent to Γ).

5.1. An identity.

We exploit the following result in our method.

PROPOSITION 5.1. *If Γ is C^2, then at every point of Γ, there holds*

$$\nabla_\Gamma \nabla_\Gamma \mathrm{id}_\Gamma^k = -\nu^k [\nabla_\Gamma \boldsymbol{\nu}] \quad \text{for } k = 1, 2, 3, \tag{5.1}$$

where k is the component index, i.e., $\mathrm{id}_\Gamma^k(\mathbf{x}) = x^k$ and $\boldsymbol{\nu} = \left(\nu^1, \nu^2, \nu^3\right)^T$.

Proof. Let $\{U, \boldsymbol{\chi}\}$ be a local chart such that the open set $\Upsilon := \boldsymbol{\chi}(U)$ is contained in Γ. Without loss of generality, we derive the identity on Υ only. Furthermore, since $\nabla_\Gamma \nabla_\Gamma$, $\boldsymbol{\nu}$, and $\nabla_\Gamma \boldsymbol{\nu}$ are independent of the parametrization, we take advantage of a particular choice and assume $\boldsymbol{\chi}$ has the form $\boldsymbol{\chi} = (\chi^1, \chi^2, \chi^3)$ with

$$\chi^1(u^1, u^2) = u^1, \quad \chi^2(u^1, u^2) = u^2, \quad \chi^3(u^1, u^2) = h(u^1, u^2), \tag{5.2}$$

where $h \in C^2$ is a height function. With this, the metric, $g_{\alpha\beta}$, and its inverse, $g^{\alpha\beta}$, are given by

$$g_{\alpha\beta} = \delta_{\alpha\beta} + (\partial_\alpha h)(\partial_\beta h), \quad g^{\alpha\beta} = \delta^{\alpha\beta} - \frac{(\partial_\alpha h)(\partial_\beta h)}{1 + (\partial_\mu h)^2}, \tag{5.3}$$

which then yields the following simplified form of the Christoffel symbols Γ_{ij}^k (of the second kind) (see (SM1.1)):

$$\Gamma_{\alpha\beta}^\gamma = \frac{1}{1 + (\partial_\mu h)^2} (\partial_\gamma h)(\partial_\alpha \partial_\beta h), \quad 1 \le \alpha, \beta, \gamma \le 2. \tag{5.4}$$

Let $\mathbf{e}_\alpha = \partial_\alpha \boldsymbol{\chi}$ for $\alpha = 1, 2$. Using (SM2.3), we have that $\mathbf{e}_\alpha^T (\nabla_\Gamma \nabla_\Gamma \mathrm{id}_\Gamma^k) \mathbf{e}_\beta = (\partial_\alpha \partial_\beta \chi^k) - \Gamma_{\alpha\beta}^\mu (\partial_\mu \chi^k)$, so

$$\mathbf{e}_\alpha^T \left(\nabla_\Gamma \nabla_\Gamma \mathrm{id}_\Gamma^k \right) \mathbf{e}_\beta = \begin{cases} -\left(1 + (\partial_\mu h)^2\right)^{-1} (\partial_k h)(\partial_\alpha \partial_\beta h) & \text{if } 1 \le k \le 2, \\ \left(1 + (\partial_\mu h)^2\right)^{-1} (\partial_\alpha \partial_\beta h) & \text{if } k = 3. \end{cases} \tag{5.5}$$

Next, note that the normal vector is given by

$$\boldsymbol{\nu} \circ \boldsymbol{\chi} = \frac{(-\partial_1 h, -\partial_2 h, 1)}{(1 + (\partial_\mu h)^2)^{1/2}}. \tag{5.6}$$

In local coordinates, $[\nabla_\Gamma \boldsymbol{\nu}] \circ \boldsymbol{\chi} = (\partial_\omega \boldsymbol{\nu}) g^{\omega\theta} (\partial_\theta \boldsymbol{\chi})^T$ by (SM2.2), so then

$$\begin{aligned} \mathbf{e}_\alpha^T [\nabla_\Gamma \boldsymbol{\nu}] \mathbf{e}_\beta &= (\partial_\alpha \boldsymbol{\chi}) \cdot (\partial_\omega \boldsymbol{\nu}) g^{\omega\theta} (\partial_\theta \boldsymbol{\chi}) \cdot (\partial_\beta \boldsymbol{\chi}) = -(\partial_\omega \partial_\alpha \boldsymbol{\chi}) \cdot \boldsymbol{\nu} g^{\omega\theta} g_{\theta\beta} \\ &= -(\partial_\alpha \partial_\beta \boldsymbol{\chi}) \cdot \boldsymbol{\nu} = -(\partial_\alpha \partial_\beta h) \nu^3 = -\frac{\partial_\alpha \partial_\beta h}{(1 + (\partial_\mu h)^2)^{1/2}}, \end{aligned} \tag{5.7}$$

which implies that

$$\mathbf{e}_\alpha^T \left(\nu^k [\nabla_\Gamma \boldsymbol{\nu}] \right) \mathbf{e}_\beta = \begin{cases} \left(1 + (\partial_\mu h)^2\right)^{-1} (\partial_k h)(\partial_\alpha \partial_\beta h) & \text{if } 1 \le k \le 2, \\ -\left(1 + (\partial_\mu h)^2\right)^{-1} (\partial_\alpha \partial_\beta h) & \text{if } k = 3. \end{cases} \tag{5.8}$$

Thus, for each $k = 1, 2, 3$,

$$\mathbf{e}_\alpha^T \left(\nu^k [\nabla_\Gamma \boldsymbol{\nu}] + \nabla_\Gamma \nabla_\Gamma \mathrm{id}_\Gamma^k \right) \mathbf{e}_\beta = 0 \text{ for } 1 \le \alpha, \beta \le 2. \tag{5.9}$$

Since $\{\mathbf{e}_1, \mathbf{e}_2\}$ spans the tangent space, and both $\nabla_\Gamma \boldsymbol{\nu}$ and $\nabla_\Gamma \nabla_\Gamma \mathrm{id}_\Gamma^k$ are tangential tensors, we obtain (5.1). ∎

5.2. The scheme. The first step in the method is to approximate the surface Hessian of id_Γ. For the convergence analysis, we assume Γ is C^{r+3} (cf. Theorem 4.3), where $r \ge 0$ is the degree of the HHJ space. This implies that $\mathrm{id}_\Gamma \in [W^{r+3,\infty}(\Gamma)]^3$,

which means $\boldsymbol{\sigma}^k := \nabla_\Gamma \nabla_\Gamma \mathrm{id}_\Gamma^k \in W^{r+1,\infty}(\Gamma; \mathbf{S})$, for $k = 1, 2, 3$. Upon recalling (3.12), a direct calculation shows that

$$a\left(\boldsymbol{\sigma}^k, \boldsymbol{\varphi}\right) + b_h\left(\boldsymbol{\varphi}, \mathrm{id}_\Gamma^k\right) = \left(\varphi^{\mathrm{nn}}, \boldsymbol{n} \cdot \nabla_\Gamma \mathrm{id}_\Gamma^k\right)_{\Sigma_{\mathrm{c}}}, \ \forall \boldsymbol{\varphi} \in \mathcal{V}_h, \ \text{ for } k = 1, 2, 3. \tag{5.10}$$

Thus, we take id_Γ^k as given data, and $\boldsymbol{\sigma}^k$ is the $L^2(\Gamma)$ projection of $\nabla_\Gamma \nabla_\Gamma \mathrm{id}_\Gamma^k$. Indeed, (5.10) comes from replacing $\boldsymbol{\sigma}$ in (3.12) with $\boldsymbol{\sigma}^k$ and replacing w, g with id_Γ^k. In addition, we have $\boldsymbol{\rho}^k \in W^{r+1,\infty}(\Gamma; \mathbf{S})$, such that the conormal-conormal moment satisfies $\boldsymbol{n}^T \boldsymbol{\sigma}^k \boldsymbol{n} = \boldsymbol{n}^T \boldsymbol{\rho}^k \boldsymbol{n}$ on Σ_{s}.

The fully discrete method is as follows. Let $\hat{\boldsymbol{\rho}}_h^k$ be given by $\hat{\boldsymbol{\rho}}_h^k := \mathrm{B}_h^m \widetilde{\boldsymbol{\rho}}^k$, with $\widetilde{\boldsymbol{\rho}}^k$ satisfying $\boldsymbol{\rho}^k \circ \boldsymbol{\Psi}^m = \mathrm{Piola}(\tilde{\boldsymbol{\rho}}^k)$, and $\mathrm{B}_h^m : H_h^0(\Gamma^m) \to V_h^m$ is the projection defined by (4.10), which satisfies the following approximation properties: $\|\hat{\boldsymbol{\rho}}_h^k - \widetilde{\boldsymbol{\rho}}^k\|_{0,h,m} \leq Ch^{r+1} \|\boldsymbol{\rho}^k\|_{H^{r+1}(\Gamma)}$, and $\|\hat{\boldsymbol{\rho}}_h^k - \widetilde{\boldsymbol{\rho}}^k\|_{L^\infty(\Sigma^m)} \leq Ch^{r+1} \|\boldsymbol{\rho}^k\|_{W^{r+1,\infty}(\Gamma)}$ (cf. [3, sect. SM4.3]).

Then we let $\hat{\boldsymbol{\sigma}}_h^k = \mathring{\hat{\boldsymbol{\sigma}}}_h^k + \hat{\boldsymbol{\rho}}_h^k$ and impose that $\mathring{\hat{\boldsymbol{\sigma}}}_h^k \in V_h^m$, for $k = 1, 2, 3$, satisfies

$$a^m\left(\mathring{\hat{\boldsymbol{\sigma}}}_h^k, \hat{\boldsymbol{\varphi}}_h\right) = -a^m\left(\hat{\boldsymbol{\rho}}_h^k, \hat{\boldsymbol{\varphi}}_h\right) - b_h^m\left(\hat{\boldsymbol{\varphi}}_h, \mathrm{id}_{\Gamma^m}^k\right) + \left(\hat{\varphi}_h^{\mathrm{nn}}, \hat{\boldsymbol{n}} \cdot \tilde{\boldsymbol{\xi}}^k\right)_{\Sigma_{\mathrm{c}}^m}, \tag{5.11}$$

for all $\hat{\boldsymbol{\varphi}}_h \in V_h^m$, where $\mathrm{id}_{\Gamma^m}^k \in W_h^m$ and $\tilde{\boldsymbol{\xi}}^k := (\nabla_\Gamma \mathrm{id}_\Gamma^k) \circ \boldsymbol{\Psi}^m$. In other words, (5.11) is simply (4.9) with $\mathring{\hat{\boldsymbol{\sigma}}}_h$ replaced with $\mathring{\hat{\boldsymbol{\sigma}}}_h^k$, $\hat{\boldsymbol{\rho}}_h$ replaced by $\hat{\boldsymbol{\rho}}_h^k$, $\tilde{w}$ replaced by $\mathrm{id}_{\Gamma^m}^k$, and $\tilde{\boldsymbol{\xi}}$ replaced by $\tilde{\boldsymbol{\xi}}^k$. Note that $\tilde{w} = w \circ \boldsymbol{\Psi}^m$ and $\mathrm{id}_{\Gamma^m}^k = \mathrm{id}_\Gamma^k \circ \boldsymbol{\Psi}^m$. Similar to (4.13), we have that the discrete projection is stable: $\|\mathring{\hat{\boldsymbol{\sigma}}}_h^k\|_{0,h,m} \leq C(\|\hat{\boldsymbol{\rho}}_h^k\|_{L^2(\Gamma^m)} + \|\nabla_\Gamma \nabla_\Gamma \mathrm{id}_\Gamma^k\|_{L^2(\Gamma)})$. When $m = 1$, $r = 0$ (piecewise linear surface), curvature information is captured by the jump terms in $b_h^m(\hat{\boldsymbol{\varphi}}_h, \mathrm{id}_{\Gamma^m}^k)$, which measure the jump of the tangent space at mesh edges.

The last step in the method is to use (5.1), i.e., let $\boldsymbol{S}_h$ approximate $\nabla_\Gamma \boldsymbol{\nu}$ through

$$\boldsymbol{S}_h := -\sum_{k=1}^{3} \hat{\nu}^k \hat{\boldsymbol{\sigma}}_h^k \in L^2(\Gamma^m; \mathbf{S}^m), \tag{5.12}$$

where $\hat{\boldsymbol{\nu}} = \left(\hat{\nu}^1, \hat{\nu}^2, \hat{\nu}^3\right)$ is the unit normal vector of Γ^m. From (3.3), and the discussion in subsection 3.1, $\|\boldsymbol{\nu} \circ \boldsymbol{\Psi}^m - \hat{\boldsymbol{\nu}}\|_{L^\infty(T^m)} \leq Ch^m$. Then, by the error analysis of subsection 4.5, and the triangle inequality, we obtain Theorem 5.2.

THEOREM 5.2. *Assume $r \geq 0$ is the degree of V_h^m and that Γ is C^{r+3}. Moreover, let $\nabla_\Gamma \boldsymbol{\nu}$ be the shape operator of Γ, and let $\boldsymbol{S}_h$ be given by* (5.12). *If $m \geq r+1$, then*

$$\|\nabla_\Gamma \boldsymbol{\nu} - \boldsymbol{S}_h \circ (\boldsymbol{\Psi}^m)^{-1}\|_{L^2(\Gamma)} \leq Ch^{r+1}, \tag{5.13}$$

where $C > 0$ depends on the domain Γ and the shape regularity of the mesh.

5.3. Practical computation. Usually, we choose $m = r+1$ when implementing the method. For $r = 0$, this corresponds to piecewise linear surface triangulations and piecewise linear Lagrange space, as well as a piecewise constant HHJ space.

5.3.1. Closed surfaces. The method is simplest when posed on closed surface triangulations. In this case, $\hat{\boldsymbol{\rho}}_h^k$ and $\tilde{\boldsymbol{\xi}}^k$ are unnecessary, so (5.11) reduces to the following: find $\hat{\boldsymbol{\sigma}}_h^k \in V_h^m$, for $k = 1, 2, 3$, such that

$$a^m\left(\hat{\boldsymbol{\sigma}}_h^k, \hat{\boldsymbol{\varphi}}_h\right) = -b_h^m\left(\hat{\boldsymbol{\varphi}}_h, \mathrm{id}_{\Gamma^m}^k\right) \quad \forall\, \hat{\boldsymbol{\varphi}}_h \in V_h^m. \tag{5.14}$$

The matrix representations of $a^m(\cdot,\cdot)$ and $b_h^m(\cdot,\cdot)$ are straightforward to assemble using standard finite element software, even for $m > 1$, although the $m = 1$ case is especially simple. Indeed, the HHJ element, though not as well-known as some other elements, is implemented in several software packages, e.g., `FELICITY` [39], `FEniCS` [2], `Firedrake` [33], and `NGSolve` [37].

TABLE 1

Listing of the 2-norm condition number of the matrix A^m discussed in subsection 5.3.1. Numbers correspond to the convergence tables in the associated sections for $m = 1$; for $m = 2, 3$, the condition numbers were larger by factors of approximately 10^2 and 10^3, respectively. The number in parentheses is the condition number of $(D^m)^{-1}A^m$, where D^m is a diagonal matrix obtained by mass-lumping of A^m.

k	Subsection 6.1	Subsection 6.2	Subsection 6.3	Subsection 6.4
0	7.61E02 (4.89E02)	3.90E02 (1.80E02)	2.89E02 (2.15E01)	4.39E02 (3.13E01)
1	9.65E02 (6.93E02)	4.87E02 (2.41E02)	4.55E02 (3.80E01)	7.10E02 (6.23E01)
2	1.11E03 (8.93E02)	5.69E02 (3.04E02)	5.88E02 (5.42E01)	8.75E02 (1.01E02)
3	1.18E03 (1.05E03)	6.39E02 (3.62E02)	7.00E02 (6.74E01)	9.64E02 (1.31E02)
4	1.26E03 (1.15E03)	6.95E02 (4.05E02)	7.72E02 (7.57E01)	1.00E03 (1.53E02)

Let A^m and B^m be the matrix realizations of $a^m(\cdot,\cdot)$ and $b_h^m(\cdot,\cdot)$, respectively. Then the right-hand side of (5.14) is simply $-B^m X^k$, where X^k is a column vector containing the kth coordinate of the degrees-of-freedom of the Lagrange space W_h^m. Let S^k be the coefficient vector corresponding to $\hat{\boldsymbol{\sigma}}_h^k$. Then, one needs to solve the linear system $A^m S^k = -B^m X^k$ for S^k, which is similar to computing a standard L^2 projection.

However, the matrix A^m is slightly different from the usual mass matrix because of the mesh dependent space $H_h^0(\Gamma^m)$, i.e., because of the edge terms. Effectively, this causes the condition number of A^m to have a slight growth as the mesh size decreases. See Table 1 for a listing of the condition number of A^m in the numerical experiments.

5.3.2. Surfaces with boundary. Surfaces with boundary pose some difficulty, because extra information about the surface is needed on the boundary $\Sigma \equiv \partial\Gamma$. Applying the scheme (5.11) requires $\tilde{\boldsymbol{\xi}}^k = (\nabla_\Gamma \mathrm{id}_\Gamma^k) \circ \boldsymbol{\Psi}^m$ on Σ_{c}^m, which implies that we need a good approximation of $\nabla_\Gamma \mathrm{id}_\Gamma \equiv \boldsymbol{P} = \mathbf{I} - \boldsymbol{\nu} \otimes \boldsymbol{\nu}$ on Σ_{c} or, equivalently, a good approximation of $\boldsymbol{\nu}$ on Σ_{c}. Thus, let $\tilde{\boldsymbol{\nu}} \in [L^\infty(\Sigma_{\mathrm{c}}^m)]^3$ with the property that

$$\|\boldsymbol{\nu} - \tilde{\boldsymbol{\nu}} \circ (\boldsymbol{\Psi}^m)^{-1}\|_{L^\infty(\Sigma_{\mathrm{c}})} = O(h^{m+1/2}). \tag{5.15}$$

Note that this precludes directly using the discrete normal $\hat{\boldsymbol{\nu}}$ of Γ^m.

Next, we must account for boundary values on Σ_{s}. Let $\boldsymbol{\rho}^k \in W^{r+1,\infty}(\Gamma; \mathbf{S})$ be given by $\boldsymbol{\rho}^k := -\nu^k \nabla_\Gamma \boldsymbol{\nu} \equiv \boldsymbol{\sigma}^k$ for $k = 1, 2, 3$ (see (5.1)), and evaluate (4.10), i.e., define $\hat{\boldsymbol{\rho}}_h^k \in V_h^m$, for $k = 1, 2, 3$, as the unique solution of

$$\left(\hat{\boldsymbol{\rho}}_h^k - \widetilde{\boldsymbol{\rho}}^k, \hat{\boldsymbol{\varphi}}_h\right)_{\mathcal{T}_h^m} + \left(\hat{\boldsymbol{n}}^T[\hat{\boldsymbol{\rho}}_h^k - \widetilde{\boldsymbol{\rho}}^k]\hat{\boldsymbol{n}}, \hat{\varphi}_h^{\mathrm{nn}}\right)_{\mathcal{E}_h^m} = 0 \,\forall\, \hat{\boldsymbol{\varphi}}_h \in V_h^m, \tag{5.16}$$

where $\hat{\boldsymbol{n}}$ is the co-normal vector on Σ_{s}^m and $\tilde{\boldsymbol{\rho}}^k$ is given by $\boldsymbol{\rho}^k \circ \boldsymbol{\Psi}^m = \tilde{\boldsymbol{\rho}}^k$. Then use $\hat{\boldsymbol{\rho}}_h^k$ to enforce boundary conditions on $\hat{\boldsymbol{\sigma}}_h^k$. However, for solving the discrete problem (5.11), we only need the values of $\hat{\boldsymbol{\rho}}_h^k$ on Σ_{s}^m. Ergo, we can restrict (5.16) to a boundary integral on Σ_{s}^m. Furthermore, we can utilize a good approximation of the boundary curvature in the following sense. Let $\tilde{\kappa}_h^n \in L^\infty(\Sigma_{\mathrm{s}}^m)$ be an approximation of the *normal curvature,* in the co-normal direction $\boldsymbol{n}$, with the property that

$$\|\boldsymbol{n}^T[\nabla_\Gamma \boldsymbol{\nu}]\boldsymbol{n} - \tilde{\kappa}_h^n \circ (\boldsymbol{\Psi}^m)^{-1}\|_{L^\infty(\Sigma_{\mathrm{s}})} = O(h^m). \tag{5.17}$$

Then, we define $\hat{\boldsymbol{\rho}}_h^k \in V_h^m$, for $k = 1, 2, 3$, as the unique solution of

$$\left(\hat{\boldsymbol{n}}^T \hat{\boldsymbol{\rho}}_h^k \hat{\boldsymbol{n}}, \hat{\boldsymbol{n}}^T \hat{\boldsymbol{\varphi}}_h \hat{\boldsymbol{n}}\right)_{\Sigma_{\mathrm{s}}^m} = -\left(\hat{\nu}^k \tilde{\kappa}_h^n, \hat{\boldsymbol{n}}^T \hat{\boldsymbol{\varphi}}_h \hat{\boldsymbol{n}}\right)_{\Sigma_{\mathrm{s}}^m} \,\forall\, \hat{\boldsymbol{\varphi}}_h \in V_h^m, \tag{5.18}$$

where we use the discrete normal $\hat{\boldsymbol{\nu}}$ of Γ^m and we set all degrees-of-freedom of $\hat{\boldsymbol{\rho}}_h^k$ not on Σ_{s}^m to zero. Note that the matrix realization of the left-hand side of (5.18) is block diagonal, where each block corresponds to an edge of Σ_{s}^m; hence, (5.18) is a trivial linear system to solve.

We now summarize the method. Let $\hat{\boldsymbol{\rho}}_h^k$ be given by (5.18) and $\tilde{\boldsymbol{\nu}}$ satisfy (5.15). Then, find $\mathring{\hat{\boldsymbol{\sigma}}}_h^k \in V_h^m$, for $k = 1, 2, 3$, such that

$$a^m\left(\mathring{\hat{\boldsymbol{\sigma}}}_h^k, \hat{\boldsymbol{\varphi}}_h\right) = -a^m\left(\hat{\boldsymbol{\rho}}_h^k, \hat{\boldsymbol{\varphi}}_h\right) - b_h^m\left(\hat{\boldsymbol{\varphi}}_h, \mathrm{id}_{\Gamma^m}^k\right) + \left(\hat{\varphi}_h^{\mathrm{nn}}, \hat{n}^k - (\hat{\boldsymbol{n}} \cdot \tilde{\boldsymbol{\nu}})\tilde{\nu}^k\right)_{\Sigma_{\mathrm{c}}^m} \tag{5.19}$$

for all $\hat{\boldsymbol{\varphi}}_h \in V_h^m$. Then, set $\hat{\boldsymbol{\sigma}}_h^k := \mathring{\hat{\boldsymbol{\sigma}}}_h^k + \hat{\boldsymbol{\rho}}_h^k$ and define $\boldsymbol{S}_h := -\hat{\nu}^k \hat{\boldsymbol{\sigma}}_h^k$.

THEOREM 5.3. *Adopt the hypothesis of Theorem* 5.2*, but let* $\boldsymbol{S}_h$ *be computed by the scheme in* (5.19)*. If* $m \geq r+1$*, then*

$$\|\nabla_\Gamma \boldsymbol{\nu} - \boldsymbol{S}_h \circ (\boldsymbol{\Psi}^m)^{-1}\|_{L^2(\Gamma)} \leq C h^{r+1}, \tag{5.20}$$

where $C > 0$ *depends on the domain* Γ *and the shape regularity of the mesh.*

Note that, by the properties of the projection and the HHJ interpolant (see subsection 4.2), we have $\|\hat{\boldsymbol{\rho}}_h^k - \widetilde{\boldsymbol{\rho}}^k\|_{L^\infty(\Sigma^m)} \leq C h^{r+1} \|\boldsymbol{\rho}^k\|_{W^{r+1,\infty}(\Gamma)}$ (cf. [3, sect. SM4.3]).

Remark 5.4. The partition of the boundary, $\Sigma = \overline{\Sigma_{\mathrm{c}}} \cup \overline{\Sigma_{\mathrm{s}}}$, depends on the geometric information available at the boundary. One can have $\Sigma \equiv \Sigma_{\mathrm{c}}$, or $\Sigma \equiv \Sigma_{\mathrm{s}}$, or a combination, so the method has some flexibility.

6. Numerical results. We present numerical results for several different domains, both with and without boundary. The discrete domains were generated by either interpolating charts on a sequence of uniformly refined grids or by creating an initial piecewise linear triangulation of the implicit, closed surface (using [38]) and interpolating the closest point map. As above, the finite element spaces V_h and W_h are of degree r and $r+1$, respectively, where $r \geq 0$, and the geometric approximation degree is denoted m, and satisfies $m = r+1$. All computations were done with the MATLAB/C++ finite element toolbox `FELICITY` [39], where we used the "backslash" command in MATLAB to solve the linear systems.

From (4.14), recall that $\boldsymbol{F}^m := \mathcal{I}_h^{1,m} \boldsymbol{\Psi}^1$, which is possible to implement, but inconvenient. Instead, we first compute $\boldsymbol{F}^{m+1}$ by standard nodal interpolation, then we define $\boldsymbol{F}^m := \mathcal{I}_h^{1,m} \boldsymbol{F}^{m+1}$, which is easy to implement over the piecewise linear triangulation of Γ^1 since it only involves simple local weighted averages and does not affect the accuracy. Indeed, this can be done by defining various forms involving dG spaces on the mesh skeleton within the finite element software.

As for the boundary data, $\boldsymbol{\nu}$ and $\nabla_\Gamma \boldsymbol{\nu}$ are known through the exact surface geometry. Moreover, these functions are easily extended away from the surface by analytic continuation. Thus, we use $\tilde{\boldsymbol{\nu}} := I_h^m \boldsymbol{\nu}$ and $\tilde{\kappa}_h^n := \hat{\boldsymbol{n}}^T \left(I_h^m[\nabla_\Gamma \boldsymbol{\nu}]\right) \hat{\boldsymbol{n}}$, where $I_h^m : H_h^2(\Gamma^m) \to W_h^m$ (different from $\mathcal{I}_h^m$) is the standard, pointwise, nodal interpolant onto W_h^m. Note that when $m = 1$, then $I_h^1 \equiv \mathcal{I}_h^{1,1}$.

In order to illustrate the effectiveness of the method, we compute the following errors: $\|I_h^m(\boldsymbol{\nu} \circ \boldsymbol{\Psi}^m) - \hat{\boldsymbol{\nu}}\|_{L^2(\Gamma^m)}$, $\|I_h^m[(\nabla_\Gamma \boldsymbol{\nu}) \circ \boldsymbol{\Psi}^m] - \boldsymbol{S}_h\|_{L^2(\Gamma^m)}$, $\|I_h^m[(\nabla_\Gamma \boldsymbol{\nu}) \circ \boldsymbol{\Psi}^m] - \boldsymbol{S}_h\|_{L^\infty(\Gamma^m)}$, $\|I_h^m(\kappa^a \circ \boldsymbol{\Psi}^m) - \kappa_h^a\|_{L^2(\Gamma^m)}$, $\|I_h^m(\kappa^g \circ \boldsymbol{\Psi}^m) - \kappa_h^g\|_{L^2(\Gamma^m)}$, where $\kappa^a = \kappa^1 + \kappa^2$ (additive curvature), $\kappa^g = \kappa^1 \cdot \kappa^2$ (Gauss curvature), and

$$\kappa_h^a := \operatorname{tr} \boldsymbol{S}_h, \quad \kappa_h^g := \det\left[\boldsymbol{S}_h + \hat{\boldsymbol{\nu}} \otimes \hat{\boldsymbol{\nu}}\right]. \tag{6.1}$$

Again, the geometric information is extended away from the surface by analytic continuation. These errors can be related to the ones in (5.13), (5.20) by equivalence

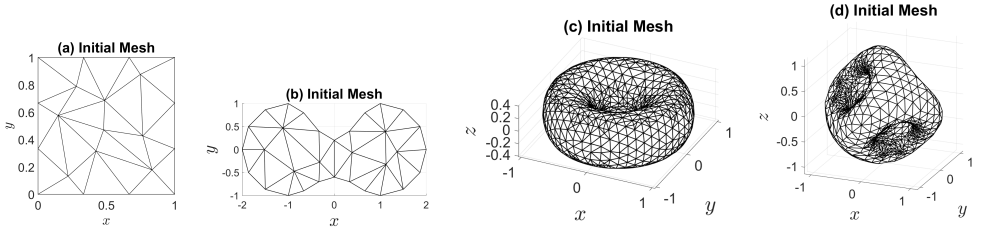

FIG. 2. *All initial meshes.* (a), (b) *These meshes are uniformly refined twice to give the* $k=0$ *case in Tables* 2 *and* 3. (c), (d) *These meshes correspond to the* $k=0$ *case in Tables* 4 *and* 5.

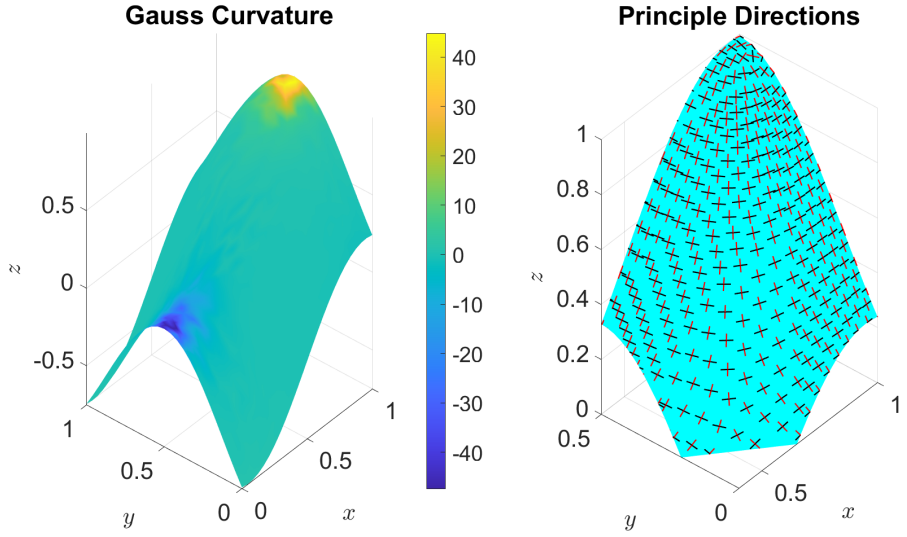

FIG. 3. *Illustration of the saddle surface in subsection* 6.1 *corresponding to* $m=1$ *and* $k=1$ *in Table* 2. *Left: color corresponds to the discrete Gauss curvature* κ_h^g. *Right: zoom-in of the surface where line segments indicate the principle directions of the surface, i.e., red (black) is* $\mathbf{d}_1$ ($\mathbf{d}_2$), *which correspond to the minimum (maximum) curvature direction.*

of norms and a triangle inequality. The estimated order of convergence (EOC) is computed by using the ratio of the error between two successive uniform refinements.

In order to avoid spurious results in the numerical convergence tests, the meshes in the examples were generated from the nonuniform/nonsymmetric meshes shown in Figure 2. The condition numbers of the "mass" matrix to invert in projecting to the HHJ space are listed in Table 1.

6.1. Saddle surface on a square. The domain is given by $(U,\boldsymbol{\chi})$, where $U=[0,1]\times[0,1]$ is the unit square and $\boldsymbol{\chi}(u^1,u^2)=(u^1,u^2,0.5(\sin(3.5(u^1-0.5))+\cos(4.2(u^2-0.5))))$. Figure 3 shows the surface with curvature data obtained from the discrete approximation. Table 2 shows the convergence behavior for the case of clamped boundary data (i.e., using $\tilde{\boldsymbol{\nu}}$), which confirms the error estimate in (5.20).

6.2. Wavy dumbbell. The domain is given by $(U,\boldsymbol{\chi})$, where the boundary of U is piecewise parametrized by

TABLE 2

Convergence errors for the saddle surface (subsection 6.1) using clamped boundary data; EOC is shown in parentheses. The number of triangles in the mesh is $N_T = 448 \cdot 4^k$, where k is the refinement index. Cases are shown for $m = 1, 2, 3$, where m is the polynomial degree of the geometry.

k	L^2 error: $\boldsymbol{\nu}$	L^2 error: $\nabla_\Gamma \boldsymbol{\nu}$	L^∞ error: $\nabla_\Gamma \boldsymbol{\nu}$	L^2 error: κ^a	L^2 error: κ^g
	$m = 1$:				
0	1.09E-01 (1.02)	1.04E 00 (0.84)	1.13E 00 (1.77)	5.94E-01 (0.89)	2.48E 00 (1.02)
1	5.44E-02 (1.01)	5.48E-01 (0.92)	4.45E-01 (1.35)	3.09E-01 (0.94)	1.26E 00 (0.97)
2	2.72E-02 (1.00)	2.81E-01 (0.96)	2.31E-01 (0.95)	1.57E-01 (0.97)	6.44E-01 (0.97)
3	1.36E-02 (1.00)	1.42E-01 (0.98)	1.27E-01 (0.86)	7.97E-02 (0.98)	3.26E-01 (0.98)
4	6.79E-03 (1.00)	7.15E-02 (0.99)	6.65E-02 (0.94)	4.02E-02 (0.99)	1.64E-01 (0.99)
	$m = 2$:				
0	3.87E-03 (2.19)	1.52E-01 (1.87)	8.89E-01 (0.94)	9.77E-02 (1.78)	4.69E-01 (1.57)
1	9.13E-04 (2.08)	3.71E-02 (2.03)	2.83E-01 (1.65)	2.49E-02 (1.97)	1.23E-01 (1.93)
2	2.25E-04 (2.02)	9.07E-03 (2.03)	8.35E-02 (1.76)	6.10E-03 (2.03)	3.08E-02 (2.00)
3	5.59E-05 (2.01)	2.25E-03 (2.01)	2.14E-02 (1.96)	1.51E-03 (2.01)	7.68E-03 (2.00)
4	1.40E-05 (2.00)	5.62E-04 (2.00)	5.41E-03 (1.99)	3.77E-04 (2.00)	1.92E-03 (2.00)
	$m = 3$:				
0	1.20E-04 (3.51)	1.41E-02 (2.95)	2.00E-01 (2.56)	1.08E-02 (2.72)	5.10E-02 (2.81)
1	1.15E-05 (3.38)	1.86E-03 (2.93)	2.12E-02 (3.24)	1.50E-03 (2.85)	7.47E-03 (2.77)
2	1.28E-06 (3.16)	2.37E-04 (2.97)	1.77E-03 (3.58)	1.92E-04 (2.97)	9.68E-04 (2.95)
3	1.55E-07 (3.05)	2.98E-05 (2.99)	2.20E-04 (3.01)	2.42E-05 (2.99)	1.22E-04 (2.99)
4	1.92E-08 (3.01)	3.73E-06 (3.00)	2.73E-05 (3.01)	3.03E-06 (3.00)	1.53E-05 (3.00)

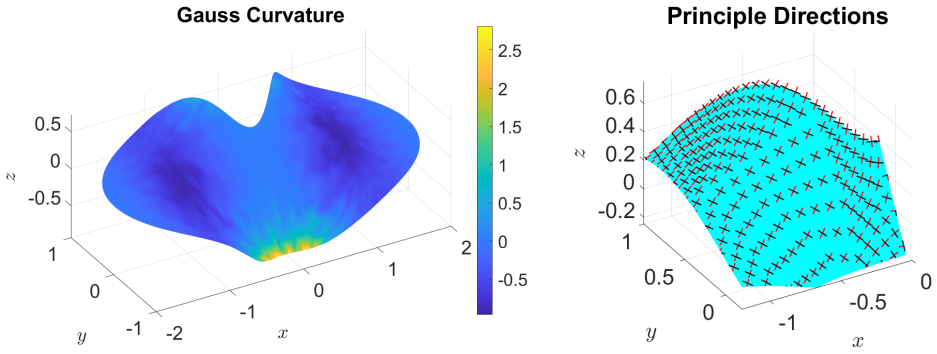

FIG. 4. *Illustration of the wavy dumbbell in subsection 6.2 corresponding to $m = 1$ and $k = 1$ in Table 3. The format is similar to Figure 3. Right figure is zoomed in on the top, curved edge of the surface.*

$$(x(t), y(t)) = \begin{cases} (\cos(t) + 1, \sin(t)) & \text{if } -\pi/2 \le t \le \pi/2, \\ (-t + 1, 0.6 + 0.4\cos(\pi t)) & \text{if } 0 \le t \le 2, \\ (\cos(t) - 1, \sin(t)) & \text{if } \pi/2 \le t \le 3\pi/2, \\ (t - 1, -(0.8 + 0.2\cos(\pi t))) & \text{if } 0 \le t \le 2. \end{cases} \tag{6.2}$$

The surface parametrization is given by $\boldsymbol{\chi}(u, v) = (u, v, e^{-u^2}\sin(2v))$. The curved element mapping is composed from two maps (recall (4.14)). The first map is a Lenoir type map [27] described in [3] that creates a curved triangulation that optimally approximates U; the second map is the parametrization $\boldsymbol{\chi}$. We then apply (4.14) to the composed map.

Figure 4 shows the surface with curvature data obtained from the discrete approximation. Table 3 shows the convergence behavior for the case of simply supported boundary data (i.e., using $\tilde{\kappa}_h^n$), which confirms the error estimate in (5.20).

TABLE 3

Convergence errors for the wavy dumbbell (subsection 6.2) using simply supported boundary data (similar format as Table 2). The number of triangles in the mesh is $N_T = 608 \cdot 4^k$, where k is the refinement index.

k	$\|\boldsymbol{\nu}_h\|_{L^2}$	$\|\boldsymbol{S}_h\|_{L^2}$	$\|\boldsymbol{S}_h\|_{L^\infty}$	$\|H_h\|_{L^2}$	$\|K_h\|_{L^2}$
	$m=1$:				
0	1.65E-01 (1.00)	5.62E-01 (0.95)	4.37E-01 (1.01)	3.67E-01 (1.01)	4.05E-01 (1.01)
1	8.25E-02 (1.00)	2.86E-01 (0.97)	2.13E-01 (1.04)	1.84E-01 (1.00)	2.05E-01 (0.98)
2	4.12E-02 (1.00)	1.44E-01 (0.99)	1.00E-01 (1.09)	9.22E-02 (1.00)	1.04E-01 (0.98)
3	2.06E-02 (1.00)	7.23E-02 (0.99)	4.79E-02 (1.06)	4.63E-02 (1.00)	5.22E-02 (0.99)
4	1.03E-02 (1.00)	3.62E-02 (1.00)	2.33E-02 (1.04)	2.32E-02 (1.00)	2.62E-02 (1.00)
	$m=2$:				
0	8.31E-03 (2.00)	3.79E-02 (1.99)	1.08E-01 (1.62)	2.35E-02 (2.04)	2.81E-02 (2.00)
1	2.07E-03 (2.01)	9.41E-03 (2.01)	2.78E-02 (1.95)	5.68E-03 (2.05)	6.95E-03 (2.01)
2	5.16E-04 (2.00)	2.34E-03 (2.01)	6.60E-03 (2.08)	1.39E-03 (2.03)	1.73E-03 (2.01)
3	1.29E-04 (2.00)	5.83E-04 (2.00)	1.55E-03 (2.09)	3.45E-04 (2.01)	4.30E-04 (2.01)
4	3.22E-05 (2.00)	1.46E-04 (2.00)	3.69E-04 (2.07)	8.59E-05 (2.01)	1.07E-04 (2.00)
	$m=3$:				
0	3.92E-04 (3.04)	3.78E-03 (2.83)	1.30E-02 (2.42)	2.12E-03 (2.72)	2.64E-03 (2.84)
1	4.85E-05 (3.02)	4.94E-04 (2.93)	2.26E-03 (2.53)	2.95E-04 (2.85)	3.49E-04 (2.92)
2	6.04E-06 (3.01)	6.28E-05 (2.98)	3.29E-04 (2.78)	3.83E-05 (2.94)	4.46E-05 (2.97)
3	7.53E-07 (3.00)	7.88E-06 (2.99)	4.42E-05 (2.89)	4.85E-06 (2.98)	5.60E-06 (2.99)
4	9.41E-08 (3.00)	9.87E-07 (3.00)	5.72E-06 (2.95)	6.09E-07 (2.99)	7.01E-07 (3.00)

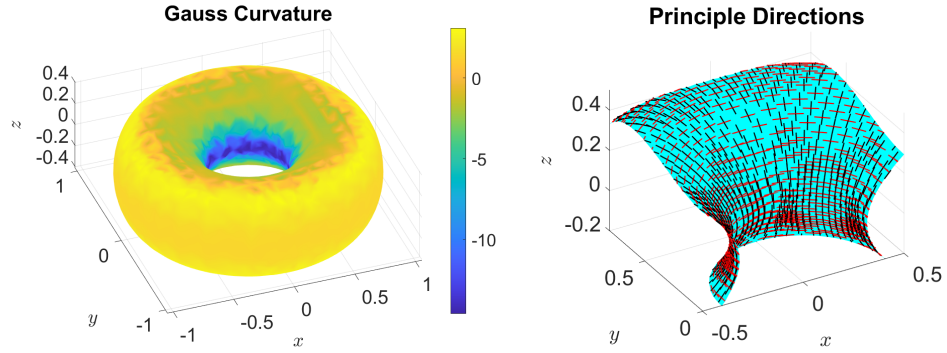

FIG. 5. *Illustration of the torus in subsection 6.3 corresponding to $m=1$ and $k=1$ in Table 4. The format is similar to Figure 3. Right figure is zoomed in on the inner hole region.*

6.3. Torus. The domain is a torus described by the zero level set of the function: $b(x,y,z) = (x^2+y^2-(6/10))^2 + (3/2)z^2 - (1/4)$. The parameterization is built from the closest point map. Figure 5 shows the surface with curvature data obtained from the discrete approximation. Table 4 shows the convergence behavior, which confirms the error estimate in (5.13).

6.4. A genus-3 surface. The domain is a closed surface described by the zero level set of the function:

$$
\begin{aligned}
b(x,y,z) &= (a_0x-2)^2(a_0x+2)^2 + (a_0y-2)^2(a_0y+2)^2 \\
&\quad + (a_0z-2)^2(a_0z+2)^2 + 3a_0^4(x^2y^2+x^2z^2+y^2z^2) \\
&\quad + 6a_0^3xyz - 10a_0^2(x^2+y^2+z^2) + 11.5,
\end{aligned} \tag{6.3}
$$

TABLE 4
Convergence errors for the torus (subsection 6.3) (similar format as Table 2). The number of triangles in the mesh is $N_T = 1904 \cdot 4^k$, where k is the refinement index.

k	$\|\boldsymbol{\nu}_h\|_{L^2}$	$\|\boldsymbol{S}_h\|_{L^2}$	$\|\boldsymbol{S}_h\|_{L^\infty}$	$\|H_h\|_{L^2}$	$\|K_h\|_{L^2}$
	$m=1$:				
0	3.16E-01 (0.00)	2.03E 00 (0.00)	6.05E-01 (0.00)	1.05E 00 (0.00)	2.55E 00 (0.00)
1	1.59E-01 (1.00)	1.07E 00 (0.92)	3.80E-01 (0.67)	5.58E-01 (0.91)	1.41E 00 (0.85)
2	7.93E-02 (1.00)	5.54E-01 (0.96)	1.81E-01 (1.07)	2.97E-01 (0.91)	7.54E-01 (0.91)
3	3.97E-02 (1.00)	2.81E-01 (0.98)	1.01E-01 (0.84)	1.56E-01 (0.94)	3.90E-01 (0.95)
4	1.98E-02 (1.00)	1.42E-01 (0.99)	5.25E-02 (0.94)	7.98E-02 (0.96)	1.99E-01 (0.97)
	$m=2$:				
0	1.76E-02 (0.00)	1.98E-01 (0.00)	3.24E-01 (0.00)	1.60E-01 (0.00)	3.70E-01 (0.00)
1	4.35E-03 (2.01)	4.94E-02 (2.00)	1.04E-01 (1.64)	4.21E-02 (1.93)	9.95E-02 (1.89)
2	1.08E-03 (2.00)	1.23E-02 (2.01)	3.29E-02 (1.66)	1.06E-02 (1.98)	2.58E-02 (1.95)
3	2.71E-04 (2.00)	3.08E-03 (2.00)	8.54E-03 (1.95)	2.67E-03 (1.99)	6.54E-03 (1.98)
	$m=3$:				
0	5.06E-03 (0.00)	3.96E-02 (0.00)	5.69E-02 (0.00)	2.82E-02 (0.00)	5.79E-02 (0.00)
1	6.64E-04 (2.93)	5.12E-03 (2.95)	1.10E-02 (2.38)	3.64E-03 (2.96)	6.77E-03 (3.10)
2	8.38E-05 (2.99)	6.46E-04 (2.99)	1.63E-03 (2.75)	4.60E-04 (2.99)	8.30E-04 (3.03)
3	1.05E-05 (3.00)	8.10E-05 (2.99)	2.14E-04 (2.93)	5.78E-05 (2.99)	1.03E-04 (3.01)

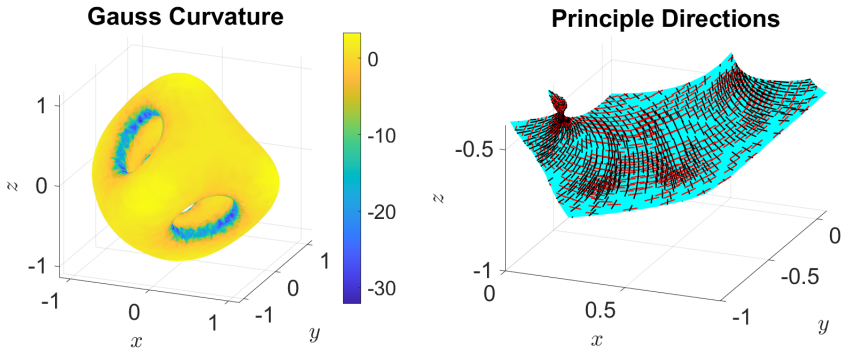

FIG. 6. *Illustration of the genus-3 surface in subsection 6.4 corresponding to $m=1$ and $k=1$ in Table 5. The format is similar to Figure 3. Right figure is zoomed in on the edge of the right hole.*

where $a_0 = 3.25$. The parameterization is built from the closest point map. Figure 6 shows the surface with curvature data obtained from the discrete approximation. Table 5 shows the convergence behavior, which confirms the error estimate in (5.13).

7. Conclusion. We have presented an effective finite element technique that can postprocess a scalar Lagrange finite element function on a discrete surface to produce an accurate approximation of the surface Hessian of the function. The method is straightforward and does not require any ad hoc modifications. The intuition behind the method is that Hessian information is obtained by looking at neighboring elements, especially for piecewise linear surfaces. This is automatically handled by the mixed FEM through the jump terms in the $b_h(\cdot,\cdot)$ bilinear form.

Furthermore, the method is directly applicable to computing convergent approximations of the full shape operator of the underlying surface (even piecewise linear triangulations) by setting the scalar function to the identity map of the discrete surface. The method may be applied to any given degree m surface, regardless of where it

TABLE 5

Convergence errors for the genus-3 surface (subsection 6.4) (similar format as Table 2). The number of triangles in the mesh is $N_T = 2808 \cdot 4^k$, where k is the refinement index.

k	$\|\boldsymbol{\nu}_h\|_{L^2}$	$\|\boldsymbol{S}_h\|_{L^2}$	$\|\boldsymbol{S}_h\|_{L^\infty}$	$\|H_h\|_{L^2}$	$\|K_h\|_{L^2}$
	$m = 1$:				
0	5.77E-01 (0.00)	4.44E 00 (0.00)	2.06E 00 (0.00)	1.88E 00 (0.00)	9.14E 00 (0.00)
1	2.93E-01 (0.98)	2.39E 00 (0.89)	1.04E 00 (0.99)	1.15E 00 (0.72)	4.79E 00 (0.93)
2	1.47E-01 (0.99)	1.24E 00 (0.95)	5.95E-01 (0.80)	6.46E-01 (0.83)	2.62E 00 (0.87)
3	7.36E-02 (1.00)	6.34E-01 (0.97)	2.95E-01 (1.01)	3.44E-01 (0.91)	1.39E 00 (0.91)
4	3.68E-02 (1.00)	3.20E-01 (0.99)	1.42E-01 (1.06)	1.78E-01 (0.95)	7.12E-01 (0.97)
5	1.84E-02 (1.00)	1.61E-01 (0.99)	7.00E-02 (1.02)	9.03E-02 (0.98)	3.58E-01 (0.99)
	$m = 2$:				
0	4.37E-02 (0.00)	1.35E 00 (0.00)	2.43E 00 (0.00)	1.13E 00 (0.00)	7.05E 00 (0.00)
1	1.14E-02 (1.94)	3.51E-01 (1.94)	7.41E-01 (1.71)	2.77E-01 (2.02)	1.73E 00 (2.03)
2	2.85E-03 (2.00)	8.74E-02 (2.01)	2.58E-01 (1.52)	6.70E-02 (2.05)	4.19E-01 (2.04)
3	7.14E-04 (2.00)	2.17E-02 (2.01)	7.10E-02 (1.86)	1.63E-02 (2.04)	1.02E-01 (2.03)
4	1.78E-04 (2.00)	5.42E-03 (2.00)	2.05E-02 (1.79)	4.02E-03 (2.02)	2.53E-02 (2.02)
	$m = 3$:				
0	3.36E-02 (0.00)	6.03E-01 (0.00)	1.16E 00 (0.00)	3.84E-01 (0.00)	2.14E 00 (0.00)
1	4.23E-03 (2.99)	6.44E-02 (3.23)	1.74E-01 (2.75)	3.76E-02 (3.35)	2.22E-01 (3.27)
2	5.36E-04 (2.98)	7.54E-03 (3.09)	2.07E-02 (3.07)	4.48E-03 (3.07)	2.19E-02 (3.35)
3	6.73E-05 (2.99)	9.24E-04 (3.03)	2.66E-03 (2.96)	5.53E-04 (3.02)	2.37E-03 (3.21)

comes from. However, convergence is only established for a sequence of shape regular meshes (with mesh size going to zero) that interpolate the exact surface in the sense of (4.14). It is not clear whether this interpolation condition can be removed.

We emphasize that the error estimate derived here involves the surface Hessian (4.22) or shape operator (5.13), (5.20). Thus, we are limited to perturbations of the surface (or the interpolant) that are $O(h^{m+2})$ in L^∞ in order to guarantee the same convergence rate. This is because, formally speaking, computing the surface Hessian or shape operator requires *two* derivatives of the surface position, which implies that the perturbation of the error estimate is $O(h^m)$.

An important aspect of our scheme is that it solves a global problem when computing the projection onto an HHJ element, which is contrary to the methods in [30, 20, 43] that compute the mean and Gauss curvature of discrete surfaces (at a vertex) using the 1-ring neighborhood of that vertex. Our scheme is convergent for general meshes, whereas these purely local schemes are not. This also implies that one should use an iterative method when solving the HHJ projection, including preconditioning to account for the small growth in the condition number of the HHJ mass matrix (see Table 1). Finding effective preconditioners is a point of future work.

REFERENCES

[1] R. A. ADAMS AND J. J. F. FOURNIER, *Sobolev Spaces*, 2nd ed., Pure Appl. Math. 140, Elsevier, Amsterdam, 2003.

[2] M. ALNÆS, J. BLECHTA, J. HAKE, A. JOHANSSON, B. KEHLET, A. LOGG, C. RICHARDSON, J. RING, M. ROGNES, AND G. WELLS, *The FEniCS project version* 1.5, Arch. Numer. Software, 3 (2015), https://doi.org/10.11588/ans.2015.100.20553.

[3] D. N. ARNOLD AND S. W. WALKER, *The Hellan–Herrmann–Johnson method with curved elements*, SIAM J. Numer. Anal., 58 (2020), pp. 2829–2855, https://doi.org/10.1137/19M1288723.

[4] D. N. Arnold and F. Brezzi, *Mixed and nonconforming finite element methods: Implementation, postprocessing and error estimates*, ESAIM Math. Model. Numer. Anal., 19 (1985), pp. 7–32, https://doi.org/10.1051/m2an/1985190100071.
[5] I. Babuška, J. Osborn, and J. Pitkäranta, *Analysis of mixed methods using mesh dependent norms*, Math. Comp., 35 (1980), pp. 1039–1062, http://www.jstor.org/stable/2006374.
[6] A. Bac, J.-L. Mari, D. Kudelski, N.-V. Tran, S. Viseur, and M. Daniel, *Application of discrete curvatures to surface mesh simplification and feature line extraction*, Actes Rencontres CIRM, 3 (2013), pp. 31–49, https://doi.org/10.5802/acirm.53.
[7] U. Bauer, K. Polthier, and M. Wardetzky, *Uniform convergence of discrete curvatures from nets of curvature lines*, Discrete Comput. Geom., 43 (2010), pp. 798–823, https://doi.org/10.1007/s00454-009-9237-4.
[8] H. Blum and R. Rannacher, *On mixed finite element methods in plate bending analysis. Part 1: The first Herrmann scheme*, Comput. Mech., 6 (1990), pp. 221–236, https://doi.org/10.1007/BF00350239.
[9] A. I. Bobenko and B. A. Springborn, *A discrete Laplace-Beltrami operator for simplicial surfaces*, Discrete Comput. Geom., 38 (2007), pp. 740–756, https://doi.org/10.1007/s00454-007-9006-1.
[10] F. Brezzi and P. A. Raviart, *Mixed finite element methods for 4th order elliptic equations*, in Topics in Numerical Analysis III: Proceedings of the Royal Irish Academy Conference on Numerical Analysis, J. J. H. Miller, ed., Academic Press, New York, 1976, pp. 33–56.
[11] P. G. Ciarlet, *The Finite Element Method for Elliptic Problems*, 2nd ed., Classics in Appl. Math. 40, SIAM, Philadelphia, PA, 2002.
[12] A. Demlow, *Higher-order finite element methods and pointwise error estimates for elliptic problems on surfaces*, SIAM J. Numer. Anal., 47 (2009), pp. 805–827, https://doi.org/10.1137/070708135.
[13] A. Demlow and G. Dziuk, *An adaptive finite element method for the Laplace–Beltrami operator on implicitly defined surfaces*, SIAM J. Numer. Anal., 45 (2007), pp. 421–442, https://doi.org/10.1137/050642873.
[14] M. Desbrun, M. Meyer, P. Schröder, and A. H. Barr, *Implicit fairing of irregular meshes using diffusion and curvature flow*, in SIGGRAPH '99: Proceedings of the 26th Annual Conference on Computer Graphics and Interactive Techniques, ACM Press, New York, 1999, pp. 317–324, https://doi.org/10.1145/311535.311576.
[15] G. Dziuk, *Finite elements For the Beltrami operator on arbitrary surfaces*, in Partial Differential Equations and Calculus of Variations, Lecture Notes in Math. 1357, S. Hildebrandt and R. Leis, eds., Springer, Berlin, 1988, pp. 142–155, https://doi.org/10.1007/BFb0082865.
[16] G. Dziuk, *An algorithm for evolutionary surfaces*, Numer. Math., 58 (1990), pp. 603–611.
[17] G. Dziuk and C. M. Elliott, *Finite element methods for surface PDEs*, Acta Numer., 22 (2013), pp. 289–396, https://doi.org/10.1017/S0962492913000056.
[18] G. Farin, *Curves and Surfaces for CAGD: A Practical Guide*, 5th ed., Morgan Kaufmann Series in Computer Graphics, Academic Press, New York, 2002.
[19] S. Frambati, H. Barucq, H. Calandra, and J. Diaz, *Practical unstructured splines: Algorithms, multi-patch spline spaces, and some applications to numerical analysis*, J. Comput. Phys., 471 (2022), 111625, https://doi.org/10.1016/j.jcp.2022.111625.
[20] R. V. Garimella and B. K. Swartz, *Curvature Estimation for Unstructured Triangulations of Surfaces*, Technical report, Los Alamos National Laboratory, 2003.
[21] T. D. Gatzke and C. M. Grimm, *Estimating curvature on triangular meshes*, Int. J. Shape Model., 12 (2006), pp. 1–28, https://doi.org/10.1142/S0218654306000810.
[22] E. S. Gawlik, *High-order approximation of Gaussian curvature with Regge finite elements*, SIAM J. Numer. Anal., 58 (2020), pp. 1801–1821, https://doi.org/10.1137/19M1255549.
[23] X. D. Gu, W. Zeng, F. Luo, and S.-T. Yau, *Numerical computation of surface conformal mappings*, Comput. Methods Funct. Theory, 11 (2012), pp. 747–787, https://doi.org/10.1007/BF03321885.
[24] C.-J. Heine, *Isoparametric Finite Element Approximation of Curvature on Hypersurfaces*, Mathematical Institute, Freiburg University, 2004.
[25] H. Huang and U. Ascher, *Surface mesh smoothing, regularization, and feature detection*, SIAM J. Sci. Comput., 31 (2008), pp. 74–93, https://doi.org/10.1137/060676684.
[26] E. Kreyszig, *Differential Geometry*, Dover, New York, 1991.
[27] M. Lenoir, *Optimal isoparametric finite elements and error estimates for domains involving curved boundaries*, SIAM J. Numer. Anal., 23 (1986), pp. 562–580.
[28] L. Li, *Regge Finite Elements with Applications in Solid Mechanics and Relativity*, Ph.D. dissertation, University of Minnesota, 2018.

[29] Y. Li, *Recovery-based a posteriori error analysis for plate bending problems*, J. Sci. Comput., 88 (2021), 77, https://doi.org/10.1007/s10915-021-01595-9.

[30] M. Meyer, M. Desbrun, P. Schröder, and A. H. Barr, *Discrete differential-geometry operators for triangulated* 2*-manifolds*, in Visualization and Mathematics III, H.-C. Hege and K. Polthier, eds., Springer, Berlin, 2003, pp. 35–57.

[31] Y. Ohtake, A. Belyaev, and A. Pasko, *Dynamic meshes for accurate polygonization of implicit surfaces with sharp features*, in SMI '01: Proceedings of the International Conference on Shape Modeling & Applications, IEEE Computer Society, Washington, DC, 2001.

[32] Y. Ohtake, A. G. Belyaev, and I. A. Bogaevski, *Polyhedral surface smoothing with simultaneous mesh regularization*, in Proceedings of Geometric Modeling and Processing: Theory and Applications, IEEE, 2000, https://doi.org/10.1109/GMAP.2000.838255.

[33] F. Rathgeber, D. A. Ham, L. Mitchell, M. Lange, F. Luporini, A. T. T. Mcrae, G.-T. Bercea, G. R. Markall, and P. H. J. Kelly, *Firedrake: Automating the finite element method by composing abstractions*, ACM Trans. Math. Software, 43 (2016), 24, https://doi.org/10.1145/2998441.

[34] A. Razdan and M. Bae, *Curvature estimation scheme for triangle meshes using biquadratic Bézier patches*, Comput. Aided Design, 37 (2005), pp. 1481–1491, https://doi.org/10.1016/j.cad.2005.03.003.

[35] N. S. Sapidis, ed., *Designing Fair Curves and Surfaces*, SIAM, Philadelphia, 1994, https://doi.org/10.1137/1.9781611971521.

[36] R. Schneider, L. Kobbelt, and H.-P. Seidel, *Mesh fairing based on harmonic mean curvature surfaces*, in Hierarchical and Geometrical Methods in Scientific Visualization, G. Farin, B. Hamann, and H. Hagen, eds., Springer, Berlin, 2003, pp. 243–267.

[37] J. Schöberl, *C++*11 *Implementation of Finite Elements in NGSolve*, Technical report ASC-2014-30, Institute for Analysis and Scientific Computing, 2014, http://www.asc.tuwien.ac.at/∼schoeberl/wiki/publications/ngs-cpp11.pdf.

[38] S. W. Walker, *Tetrahedralization of isosurfaces with guaranteed-quality by edge rearrangement (TIGER)*, SIAM J. Sci. Comput., 35 (2013), pp. A294–A326, https://doi.org/10.1137/120866075.

[39] S. W. Walker, *FELICITY: A MATLAB/C++ toolbox for developing finite element methods and simulation modeling*, SIAM J. Sci. Comput., 40 (2018), pp. C234–C257, https://doi.org/10.1137/17M1128745.

[40] S. W. Walker, *The Kirchhoff plate equation on surfaces: The surface Hellan–Herrmann–Johnson method*, IMA J. Numer. Anal., 42 (2021), pp. 3094–3134, https://doi.org/10.1093/imanum/drab062.

[41] S. W. Walker, *Poincaré inequality for a mesh-dependent* 2*-norm on piecewise linear surfaces with boundary*, Comput. Methods Appl. Math., 22 (2022), pp. 227–243, https://doi.org/doi:10.1515/cmam-2020-0123.

[42] M. Wardetzky, M. Bergou, D. Harmon, D. Zorin, and E. Grinspun, *Discrete quadratic curvature energies*, Comput. Aided Geom. Design, 24 (2007), pp. 499–518, https://doi.org/10.1016/j.cagd.2007.07.006.

[43] Z. Xu and G. Xu, *Discrete schemes for Gaussian curvature and their convergence*, Comput. Math. Appl., 57 (2009), pp. 1187–1195, https://doi.org/10.1016/j.camwa.2009.01.024.

[44] Z. Xu, G. Xu, and J.-G. Sun, *Convergence analysis of discrete differential geometry operators over surfaces*, in Mathematics of Surfaces XI, R. Martin, H. Bez, and M. Sabin, eds., Springer, Berlin, 2005, pp. 448–457.

[45] X. Ye, T. R. Jackson, and N. M. Patrikalakis, *Geometric design of functional surfaces*, Comput. Aided Design, 28 (1996), pp. 741–752, https://doi.org/10.1016/0010-4485(95)00080-1.

[46] X. Yin, M. Jin, F. Luo, and X. D. Gu, *Discrete Curvature Flows for Surfaces and* 3*-Manifolds*, Springer, Berlin, 2009, pp. 38–74, https://doi.org/10.1007/978-3-642-00826-9_3.